Differences in behavior between surface and cave *Astyanax mexicanus* may be mediated by changes in catecholamine signaling

Kathryn Gallman[1], **Eric Fortune**[1], **Daihana Rivera**[1], **Daphne Soares**[1]
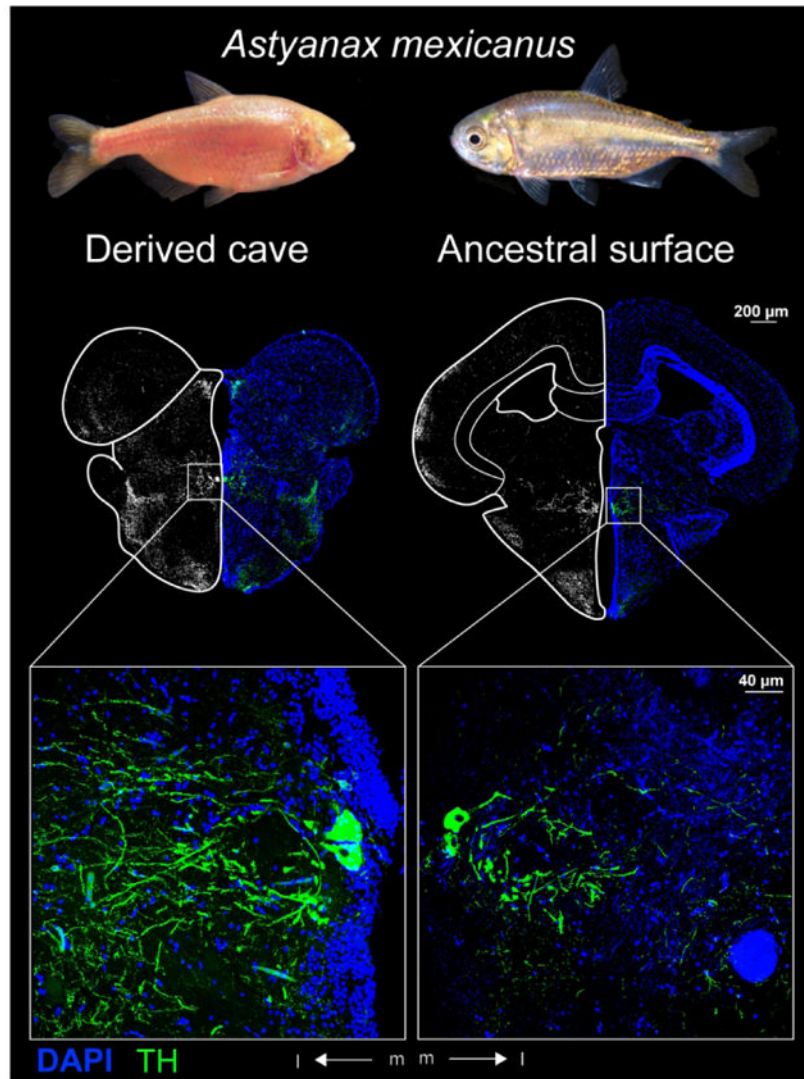
[1]Biological Sciences, New Jersey Institute of Technology, New Jersey USA 07102

Abstract

Astyanax mexicanus is a teleost fish that is in the process of allopatric speciation. Ancestral *Astyanax* are found in surface rivers and derived blind forms are found in cave systems. Adaptation to life in nutrient poor caves without predation includes the evolution of enhanced food seeking behaviors and loss of defensive responses. These behavioral adaptations may be mediated by changes in catecholaminergic control systems in the brain. We examined the distribution of tyrosine hydroxylase, a conserved precursor for the synthesis of the catecholamines dopamine and noradrenaline, in the brains of surface and cave *Astyanax* using immunohistochemistry. We found differences in tyrosine hydroxylase staining in regions that are associated with non-visual sensory perception, motor control, endocrine release, and attention. These differences included significant increases in the diameters of tyrosine hydroxylase immunoreactive soma in cave *Astyanax* in the olfactory bulb, basal telencephalon, preoptic nuclei, ventral thalamus, posterior tuberculum, and locus coeruleus. These increases in modulation by dopamine and noradrenaline likely indicate changes in behavioral control that underlie adaptations to the cave environment.

Graphical Abstract

The teleost fish *Astyanax mexicanus* is extant in an ancestral surface form (right) and derived cave forms (left). Adaptation to life in nutrient poor caves without predation increased exploratory foraging behaviors and decreased aversion to potential predatory cues in the cavefishes. Tyrosine hydroxylase immunohistochemistry revealed larger catecholaminergic neurons in regions of the cave *Astyanax* brain that may mediate these changes in behavior.

Corresponding author: Kathryn Gallman kathryn.e.gallman@njit.edu.

Astyanax mexicanus

Derived cave   Ancestral surface

200 µm

40 µm

DAPI TH   l ← m m → l

Keywords

Evolution; Adaptation; Catecholamines; Teleost fish; Dopamine; Noradrenaline; Tyrosine hydroxylase

Introduction

Foraging strategies often reflect an interaction between the abundance of food resources and predators. For example, cave habitats generally have low resource availability and few predators (Howarth, 1993; Jeffery, 2001; Fernandes et al., 2016). As a result, animals that live in caves spend more time foraging and have reduced sensitivity to predatory cues compared to species in surface environments, which generally have higher resource abundance and greater risk of predation (Wilkens & Hüppop, 1986; Gillespie & Caraco,

1987; Howarth, 1993; Brown, 1999; Protas et al., 2008; Yoshizawa et al., 2010; Duboué et al., 2011; Espinasa et al., 2014).

Both foraging and predator avoidance behaviors are regulated by catecholamine systems in the brain (Björklund & Dunnett, 2007; Duboué et al., 2011; Rosen 2017: Deslauriers et al., 2019). Catecholamines, such as dopamine (DA) and noradrenaline (NA), are primarily involved in the selection of behavioral responses to environmental stimuli (Chakravarthy et al., 2010; Wright & Panksepp, 2014). Catecholaminergic signaling mediates the selection of behavior by potentiating the perception of rewarding or stressful stimuli (Pashcel & Ninteman, 1963; Schultz, 1998; Calabresi et al., 2007; Prokopova, 2010). These stimuli can include external cues, such as food or predator detection, but may also involve homeostatic cues, such as hunger or pain. Interestingly, the subsequent behavior induced by these stimuli can, in turn, be rewarding, such as the successful consumption of food (Schultz, 1998; Calabresi et al., 2007). This results in the potentiation of the rewarding response via the action of catecholamines on neurons of motor control systems in the central nervous system (Aou et al., 1983). By potentiating both the stimulus perception and behavioral response circuitry that results in rewarding outcomes, catecholaminergic modulation can reinforce behaviors suited for survival in a given environment (Wright & Panksepp, 2014).

To investigate the role of catecholamines in the regulation of foraging behaviors and responses to potential predatory cues, we examined the brains of the teleost fish *Astyanax mexicanus,* a species that is experiencing allopatric speciation in recently invaded cave habitats (Fumey et al., 2018). Surface and cave *Astyanax* have significantly different behaviors related to the abundance of resources and predators (Protas et al., 2008; Salin et al., 2010; Yoshizawa et al., 2010; Duboué et al., 2011; Keene et al., 2015; Rétaux et al., 2015). For example, blind cave *Astyanax* continuously search for food whereas surface *Astyanax* both exhibit diurnal changes in foraging activity and use a sit-and-wait strategy in which movement is dramatically increased in the presence of food cues (Salin et al., 2010; Duboué et al., 2011). Surface *Astyanax* exhibit escape responses to novel stimuli as a mechanism for avoiding predation, whereas cave *Astyanax* actively investigate novel stimuli (Yoshizawa et al., 2010; Keene et al., 2015). This active investigation is believed to occur because of the lack of predators in the cave habitat (Yoshizawa et al., 2010; Keene et al., 2015).

To compare the catecholamine systems in surface and cave *Astyanax* brains, we examined differences in tyrosine hydroxylase immunoreactivity. Tyrosine hydroxylase (TH) is the rate limiting enzyme in the biosynthesis of the catecholamine neuromodulators of the central nervous system, DA and NA (Candy & Collet, 2005; Wall & Volkoff, 2013). We found that TH immunoreactive (THir) somata in the brains of cave *Astyanax* are significantly larger size than in surface *Astyanax* in the olfactory bulb (OB), the medial olfactory tract (MOT), the anterior and parvocellular preoptic nuclei (PPa, PPp), the suprachiasmatic nucleus (SCN), the posterior tuberculum (periventricular nucleus: TPp; paraventricular organ:PVO adjacent), and the locus coeruleus (LC). The sizes of THir labelled somata in the intermediate nucleus of the subpallium (Vi), ventromedial thalamic nucleus (VM), and the posterior tuberal nucleus (PTN) were not significantly different between surface and cave forms. Further, we found THir fibers within the optic tectum (TeO), tertiary gustatory

nucleus (TGN) and tract (TGT), hypothalamus, and other nuclei in both forms. In the secondary gustatory nucleus (SGN), we only observed THir fibers in cave *Astyanax*.

Methods

Animals:

Our study used non-breeding male and female adult specimens (approximately one year old) of surface and Pachón cave *Astyanax* (standard lengths of 4.3- 5.1 cm, n=20). Our initial breeding population was obtained from the Jefferey lab stock in 2015 and offspring were raised under a 12-hour light-dark cycle and fed once daily. All animal husbandry and experimental procedures were reviewed and approved by the Institutional Animal Care and Use Committee (IACUC) of Rutgers University Newark and follow guidelines for animal care and use established by the National Research Council and Society for Neuroscience. NJIT is under Rutgers IACUC oversight.

Tissue Preparation:

We euthanized fish via immersion in tricaine methanesulfonate salt (MS-222, 10g/L). We immediately fixed the brains by transcardial perfusion of cold heparinized saline (0.9% Sodium Chloride with heparin (20 units/mL) followed by 10% neutral buffered formalin (3.7% formaldehyde; MilliporeSigma HT501128). We removed the heads and continued fixation for 4-6 hours in the formalin solution. We transferred the brains into a sucrose solution (30% sucrose in 0.1M phosphate buffered saline, PBS) overnight at 4°C. The following day, we removed the brains from the skull and returned them to the sucrose solution at 4°C. We cut each brain into 20μm thick sections using a cryostat (ThermoFisher HM525NX) set to −20°C and mounted sections on positively charged glass slides (ThermoScientific 12460S). Sections were either processed the following day or stored at −20°C for up to one week.

Immunohistochemistry:

We washed the slides in 0.1M PBS twice for ten minutes and blocked (0.2% fetal bovine serum, 0.3% Tween 20, 10% normal goat serum in 0.1M PBS) for 2 hours at room temperature. We incubated the sections in primary antibody (TH monoclonal mouse antibody, RRID: AB_2201528) diluted 1:500 in incubation buffer (0.2% FBS, 0.3% Tween 20 in 0.1M PBS) overnight at 4°C. The following morning, we washed the sections three times for 10 minutes with 0.1M PBS and 0.1% Tween20 (PBSTween) and incubated with Alexa Fluor 594 conjugated anti-mouse secondary antibody (abcam, ab150116) diluted 1:500 in blocking solution for two hours at room temperature. We then washed three times for 10 minutes with PBSTween. Finally, we counterstained with DAPI (1:5000) for 30 minutes and washed three times for 10 minutes with 0.1M PBS before mounting with 90% glycerol in phosphate buffer.

Imaging:

We used a confocal microscope (Leica SP8) with excitation at 405 nm and 552 nm to capture immunofluorescent images. We took scans of full sections with a 20x dry objective lenses. We also took higher resolution scans using 40x and 63x oil immersion objective

lenses. We processed images using Leica LAS X confocal software (RRID: SCR_013673). We also imaged sections using an epifluorescent microscope (Olympus PX50) at 40x magnification equipped with an OMAX 18.0MP camera controlled by ToupView software (RRID: SCR_017998).

We used two strategies for visualization of the fluorescent material. We visually scanned the original THir image, which included the full range of relative signal brightness captured by the microscope. This was compared to a grayscale image with far greater contrast, almost black and white. This new thresholded image emphasized dim signal, which was useful for locating some lightly stained fiber tracts and sparsely distributed THir cells. Finally, we incorporated the DAPI signal to help determine the boundaries of brain areas. This can be seen in the photomicrographs: on the right are combined THir and DAPI images highlighting the relative densities of THir staining and Nissl staining. On the left are high contrast reflected greyscale images of the same material that highlights the weakly THir stained areas at the cost of reducing visual perception of relative density of THir labeling.

Quantification:

We sectioned five surface and five cavefish brains in the coronal plane. We measured the diameters of THir somata from the axon hillock to the farthest point of the soma through the nucleus using FIJI (Schindelin et al., 2012; RRID: SCR_002285). We measured THir somata from both epifluorescent images and confocal reconstructions. We performed Student's *t*-tests using R (R core team, 2017; RRID: SCR_001905) on log normalized measurements between *Astyanax* forms by brain nucleus and between brain nuclei of the same form. We used ggplot2 to generate plots in R (Wickham, 2016; R core team, 2017).

Results

External morphology

There were differences in external morphology of brain structures in surface and cave *Astyanax*. These differences included the shapes and sizes of the olfactory bulb (OB), telencephalon, optic tectum (TeO), hypothalamus, and cerebellum.

The OB in surface *Astyanax* appeared small and triangular shaped whereas the OB in cave *Astyanax* appeared relatively large and ellipsoid shaped (Fig 1 a, b). The dorsal edge of the pallium (dorsal telencephalic area; D) in surface *Astyanax* was dome shaped but had rostrocaudal ridges in cave *Astyanax* (Fig 1c - f). Further, there is a lateral bulge along the edge of the subpallium (ventral telencephalic area; V) in cave *Astyanax* but not surface *Astyanax* (Fig 1c-f). As expected, optic areas including the TeO, torus longitudinalis (TL), and telencephalic ventricle (TeV) were dramatically smaller in cave *Astyanax* than in surface *Astyanax* (Fig 2, 3). The dorsal edges of the TeO were dome shaped in both *Astyanax* forms, but extended farther laterally in surface *Astyanax*. At the level of the posterior tuberculum and caudally, TL appeared in the TeV ventral to medial TeO in surface *Astyanax* (Fig 2d, f; Fig 3b, d). The TL is reduced in size and appears further caudal in cave *Astyanax*, starting at the level of the commissura tecti (Ctect; Fig 3a). The TeV is dramatically reduced in cave *Astyanax* (Fig 3c).

In contrast, the hypothalamus of cave *Astyanax* appeared relatively larger than in surface *Astyanax* (Fig 3). Further, the volume of the hypothalamus is shifted rostrally in cave *Astyanax*, probably due to the atrophy of tectal areas in these fish. This can be seen by comparing the locations of the inferior lobe of the hypothalamus (IL) between the cave and surface forms (Fig 3 a-f). The extensions of the IIIrd ventricle, the posterior (PR) and lateral recesses (LR), appear larger, with a greater density of cells in Hc/Hd (caudal and dorsal zones of the periventricular hypothalamus) in the cave form (Fig 3 c, d)

The cerebellum also differed in external morphology between *Astyanax*. Similar to the dorsal edge of the pallium, the rostral cerebellum was smooth, and dome shaped in surface *Astyanax* and exhibited rostral caudal ridges in the cave *Astyanax* (Fig 4 a-d). The caudal cerebellum, however, was roughly spherical with ridges in surface *Asytanax* (Fig 4f) but was ellipsoid shaped with smoother edges in cave *Astyanax* (Fig 4e).

THir somata and fibers

We found THir somata and fibers in the OB, the telencephalon (MOT, Vi), the preoptic area (PPa, PPp, the ventromedial and ventrolateral thalamic nuclei (VM, VL), posterior tuberculum (TPp, PVO adjacent), and locus coeruleus (LC) in both *Astyanax* forms. We found no THir somata in the rhombencephalon caudal to LC, but we did not examine the brain caudal to the end of the cerebellum. THir somata had significantly (see below) larger diameters in cave *Astyanax* in the OB, MOT, PPa, PPp, SCN, VL, TPp, and LC.

THir fibers appeared in and around THir somata as well as within brain regions without THir stained cell bodies. THir fibers ran from the OB through the rostrocaudal extent of the telencephalon, from the subpallium (V) to the posterior zone of D (Dp), with contralateral projections through the ventral telencephalic commissure (Cant; Fig 5). THir fibers also lay in the preoptic region, ventral thalamus, pretectum, and in layered bands within the TeO. We also found THir fibers in the gustatory regions of the posterior tuberculum, TS, the hypothalamus, and rhombencephalon.

Olfactory bulb

THir somata were spherical and small (10 μm) in the OB of both surface and cave forms. Somata were relatively less dense in the center of the ICL, with a greater density of cells along its periphery (Fig 1a, b; Fig 6a, b). The greatest density of cells appeared dorsally on the border of the external cell layer (ECL; Fig 6a, b). Although the mean diameters of cells of OB THir somata are similar, the diameters in cave *Astyanax* (mean diameter 6.7 ± 1.2 μm; N = 3369) were nevertheless significantly larger (*t*-test; p-value < 0.001) than in surface *Astyanax* (mean diameter: 6.5 ± 1.1μm; N = 3083; Fig 6c). The largest (> 12.5) diameter THir somata only appeared in cave *Astyanax* and may represent a THir population within the OB that is not present in surface *Astyanax*. Under this assumption, we performed a second comparison of only the smaller (12.5 μm) OB THir somata diameter distributions between *Astyanax* forms. Even with the removal of this group of larger cells, OB THir somata remained significantly larger (*t*-test; p-value < 0.001) in diameter in the cave *Astyanax* (mean diameter 6.7 ± 1.1 μm; N = 3359) than in the surface *Astyanax* (mean diameter 6.5 ± 1.1 μm; N = 2971). As such, whether the OB THir somata in cave *Astyanax*

represent one population or two, they are still significantly larger in diameter than in surface *Astyanax*.

THir somata in the *Astyanax* OB resemble those of short-axon cells, also called DA preglomerular interneurons neurons (Bundschuh et al., 2012) and juxtaglomerular cells (Fuller et al., 2006), described in the zebrafish OB (Olivares & Schmachtenberg, 2019). These cells represent an intriguing avenue for future research into the differences in morphology, transmitter expression, and function across teleostean species (Alonso et al., 1989; Honaken & Ekström, 1990; Sas et al., 1990; Edwards & Michel, 2002) and compared to those in mammals (Kosaka & Kosaka, 2005; Kosaka & Kosaka, 2010; Kiyokage et al., 2010).

THir fibers in the OB appeared in the ECL and GL, with increasing fiber density at the periphery and lower density labeling in the ICL (Fig 6a, b). THir OB fibers may include projections from neurons in the ICL and ECL, as most axons appear to project towards the periphery (Fig 1: a, b; Fig 6: a, b). THir OB fibers also likely included projections from other THir brain nuclei, as a bright fiber tract connects the OB to THir fibers of the ventral telencephalon (Fig 5).

Telencephalon

The medial olfactory tract (MOT; Von Bartheld et al., 1984; Biechl et al., 2017) contained small (12 μM), spherical THir soma in both surface and cave forms. These cells lay lateral to the ventral nucleus of the subpallium (Vv) and extended dorso-laterally along the nucleus (Fig 6d, e). In surface *Astyanax* the MOT appeared as a thin arc (Fig 6e), whereas in cave *Astyanax* the MOT appeared wider and longer (Fig 6d). MOT THir somata were significantly larger (*t*-test; p-value < 0.001) in cave *Astyanax* (mean diameter 7.6 ± 1.1 μm; N = 86) than in surface *Astyanax* (mean diameter 6.4 ± 1.2 μm; N = 199; Fig 6f). THir fibers both overlapped the region of MOT with THir somata and extended medially in both forms. A few fibers also appeared within Vv and are likely projections from MOT (Fig 6d, e).

The lateral olfactory tract (LOT; Von Bartheld et al., 1984; Biechl et al., 2017) contained THir fibers but not somata (Fig 6d, e). The LOT is visually distinct in coronal sections, separated by a thin (~10-100μm wide) gap. In the surface *Astyanax* this gap in staining appeared broader than in cave *Astyanax* (Fig 1c, d; Fig 6d, e). The fibers of LOT appeared to project from the central subpallium into Dp. The LOT fibers in surface *Astyanax* extended into Dp obliquely while the LOT fibers of the cave *Astyanax* appeared to extend almost horizontally into Dp and dorsally from Dp into the lateral region of D (Dl) in cave *Astyanax* (Fig 1c, d).

THir fiber projections in the telencephalon appeared throughout its rostrocaudal extent and were often associated with THir somata. For example, the THir fibers that connect the OB to Dp can be seen in an orthogonal band running from the ventral subpallium to the pallium (Fig 5a, b).

The intermediate nucleus of the subpallium (Vi; Biechl et al., 2017) contained sparsely distributed, small (10 μm), spherical THir somata. Vi lay caudal to the telencephalic

commissures (Fig 5a) and centrally along the pallial-subpallial boundary (Fig 1e, f). THir somata appeared just dorsal and medial to the nucleus taeniae (NT; Fig 1e, f) among the lateral forebrain bundle (LFB; Fig 6g, h). Vi THir somata were not significantly different in diameter between surface (6.9 ± 1.3 μm; N = 64) and *cave Astyanax* (6.8 ± 1.5 μm; N = 61; Fig 6i).

Vi THir somata were almost indistinguishable among a dense band of THir fibers that extended along the length of the pallial/subpallial boundary, from Vp (postcommissural nucleus of V) to Dp (Fig 1e, f). In surface *Astyanax*, this band of THir extended in a thick horizontal band across the central telencephalon (Fig 1f). The THir fiber band was smaller in cave *Astyanax* and traveled more obliquely from Vp to Vi before curving to project towards Dp horizontally. There were also fibers that appear to originate in Vi and Dp that extended dorsally into the pallium in cave *Astyanax* (Fig 1e).

Preoptic Area

The anterior region of the parvocellular preoptic nucleus contained THir somata in both fish forms (Fig 1e, f). These nuclei extend laterally and dorsally from below the third ventricle in the hypothalamus in an arc that turned back towards the midline (Fig 6j, k). PPa THir somata lay ventral and medial to the THir somata in Vi (Fig 1e, f) and ran rostrocaudally along the ventral edge of the subpallium up to the caudal boundary of the telencephalon (Fig 7c). Dense clusters of PPa THir somata lay along the midline at the ventral edge of the preoptic area. There were also cells farther dorsally along the midline that appeared in lower densities (Fig 6j, k). PPa THir somata had significantly larger (*t*-test; p-value < 0.001) diameters in cave *Astyanax* (mean diameter 11.0 ± 2.4 μm; N = 364) than in surface *Astyanax* (mean diameter 9.3 ± 2.6 μm; N = 541; Fig 6l).

PPa THir fibers appeared to project dorsal-caudally towards the thalamus. In the coronal plane, this manifested as dense lines of THir fibers along the medial and lateral borders of the preoptic area with bands of THir fibers running between in an almost ladder-like formation (Fig 6j, k). The medial line of PPa THir fibers coalesced into the lateral band of THir fibers extending from Vp to Dp, but appeared to terminate in NT, just ventral to Dp (Fig 1e, f).

PPp THir somata appeared near the dorsal edge of the optic tract and can be differentiated from PPa as a smaller (p-value < 0.001) less dense cell population in both *Astyanax* forms (Fig 7c). PPp THir somata lay along the diencephalic ventricle (Div; Fig 8a, b) between the ventral thalamus (VT) and suprachiasmatic nucleus (SCN; Fig 9c) and continued ventral caudally into the medial diencephalon in a sparse band of cells (Fig 7a). PPp THir somata had significantly larger (*t*-test; p-value < 0.001) diameters in cave *Astyanax* (mean diameter 8.3 ± 1.2 μm; N = 101) than in surface *Astyanax* (mean diameter 7.8 ± 1.2 μm; N = 117; Fig 8c). Rostrocaudally, PPp THir fibers appeared in a ventral caudal projecting band from the dorsal edge of the optic tract through the diencephalon and were spaced apart and individually discernable rather than intertwined in a dense band (Fig 7a).

SCN THir somata appeared just caudal to the transition from PPa to PPp and continue in a rostrocaudal band immediately dorsal to the optic chiasm and ventral to PPp (Fig 7a).

Spherical SCN THir somata lay both near the ventricle as well as more laterally along the ventral border of the preoptic region (Fig 8a, b). SCN THir somata had significantly larger (*t*-test; p-value < 0.01) diameters in cave *Astyanax* (mean diameter 9.5 ± 2.3 μm; N = 26) than in surface *Astyanax* (mean diameter 7.9 ± 1.2 μm; N = 54; Fig 8d). SCN THir fibers projected ventrally to coalesce into a bright band of intertwined fibers that ran above the optic tract in the rostrocaudal axis (Fig 7a).

Ventral Thalamus

THir somata in the ventral thalamus (VT) lay dorsal to PPp (Fig 7a). VT consisted of two populations of THir somata, the ventral medial (VM) and ventral lateral thalamic nuclei (VL). VM THir somata lay along the ventricle, while VL THir somata lay lateral to the VM population with a discernable gap between the two cell populations (Fig 9a-c). VL THir somata were significantly larger than VM THir somata for both *Astyanax* forms (*t*-test; p-value < 0.001). VM THir somata diameters were not statistically different (*t*-test; p-value = 0.37) between cave (7.0 ± 1.5 μm; N = 79) and surface *Astyanax* (7.1 ± 1.3 μm; N = 295; Fig 9d). VL THir somata had significantly larger (*t*-test; p-value < 0.001) diameters in cave *Astyanax* (8.9 ± 2.1 μm; N = 83) than in surface *Astyanax* (7.7 ± 1.4 μm; N = 96; Fig 9e). Both VM and VL sent THir fiber projections laterally, forming a single thick band that terminated just dorsal to the lateral preglomerular nucleus (PGl; Fig 2c, d). The tertiary gustatory nucleus (TGN) also showed THir fibers in cave, but not surface *Astyanax* (Fig 2e, f).

THir somata in the periventricular pretectal nucleus (PPr) formed a densely packed cell cluster dorsal to VM and VL (Fig 2c, d) and ventral to the posterior commissure (Cpost; Fig 10a, b). PPr THir somata appeared in a densely packed cell cluster along the ventricle (Fig 10a, b). A few PPr THir somata also lay slightly laterally along Cpost (Fig 10b). PPr THir somata diameters were not statistically different (*t*-test; p-value = 0.33) between cave (mean diameter 8.2 ±1.6 μm; N = 189) and surface *Astyanax* (mean diameter 8.0 ± 1.5 μm; N = 270; Fig 10c). PPr THir somata sent projections dorsal to the fasciculus retroflexus (FR; Fig 10a, b) towards the optic tectum (TeO; Fig 2c, d). PPr THir fibers also traveled along the ventral border of the TeO before joining dorsally projecting THir fibers VT at the lateral edge of the thalamus (Fig 2c, d). THir fibers were also evident within TeO in thin layered bands in both *Astyanax* forms (Fig 11a).

Posterior tuberculum

THir somata in the posterior tuberculum began at the caudal edge of the THir VT neurons (Fig 2c, d; Fig 9a, b). In this region, THir somata in the periventricular nucleus of the posterior tuberculum (TPp) were spherical and larger (*t*-test; p-value < 0.001) than THir VT cells (Fig 9a, b). Further caudally, TPp THir somata were even larger (*t*-test; p-value < 0.001) and pear shaped (Fig 10d, e). These magnocellular cells continued ventrocaudally through the tuberal region dorsal and lateral to the paraventricular organ (PVO; Rink & Wulliman, 2001; Fig 10g, h). Following the nomenclature used by Rink & Wulliman (2001), we have designated the smaller (< 25 μm), more rostral TPp cell bodies as type 1 neurons and the more caudal and larger (< 45 μm) pear shaped TPp and PVO adjacent cell bodies as type 2 neurons.

Spherical TPp type 1 THir somata resembled those of the ventral thalamus. In the coronal plane, THir somata lined the ventricle and axon hillocks tapered in the lateral direction (Fig 9a, b). TPp type 1 THir somata diameters were significantly larger (*t*-test; p-value < 0.001) in cave *Astyanax* (mean diameter 13.8 ± 3.5 μm; N = 61) than in surface *Astyanax* (mean diameter 8.3 ± 1.5 μm; N = 50; Fig 9f). Fiber projections from TPp type 1 THir somata appeared to join those of VT as they coalesced into a laterally projecting fiber tract. Unlike VT, the more ventral position of TPp type 1 THir somata sent this fiber tract in a dome shaped arc (Fig 2c, d). Together, the VT and TPp type 1 THir fiber tracts encircled the median forebrain bundle (MFB; Fig 9a, b).

Magnocellular pear shaped TPp type 2 THir somata lay directly ventral and caudal to the Type 1 cells along the ventricle (Fig 7b). TPp type 2 THir somata had significantly larger (*t*-test; p-value < 0.001) diameters in cave *Astyanax* (mean diameter 34.0 ± 6.2 μm; N = 35) than in surface *Astyanax* (mean diameter 21.7 ± 7.0 μm; N = 35; Fig 10 f). Type 2 THir somata had relatively tick axons and sent projections in lateral tracts that encircled the MFB (Fig 10d, e) to converge near the THir fibers of the tertiary gustatory nucleus (TGN; Fig 2e, f).

We also found THir fibers in the lateral hypothalamic nucleus (LH) and IL, ventral to TPp type 2 THir somata. Fibers from LH appeared to move along the lateral border of the hypothalamus into IL. IL THir fibers also appeared to meet the ventral edge of tertiary gustatory tract (TGT), near where THir somata in the posterior tuberculum appeared to project (Fig 2e, f).

Magnocellular THir somata also lay adjacent to PVO and ventral caudal to the magnocellular THir somata of TPp (Fig 3a, b). These THir type 2 cells were significantly smaller (*t*-test; p-value < 0.001) than those of TPp in both *Astyanax* forms, which led us to represent them separately than the TPp type 2 population, although they may be one contiguous population (Forlano et al., 2014). PVO adjacent THir somata lay both lateral and ventral to the borders of PVO (Fig 10g, h) and were significantly larger (*t*-test; p-value < 0.001) in cave *Astyanax* (mean diameter of 22.8 ± 8.5 μm; N = 67) than in surface *Astyanax* (mean diameter of 15.4 ± 5.5 μm; N = 48; Fig 10i). These cells also had a distinctive semi-circle projection pattern that opened lateral to PVO (Fig 10g, h). These projections appeared to travel dorsally and laterally in the coronal plane and caudally in dorsal and ventral tracks in the sagittal plane (Fig 7d).

A group of small (12 μm), spherical THir somata in PTN (Baeuml et al., 2019) lay caudal to the PVO adjacent magnocellular cells and dorsal to PR (Fig 3c, d). Although densest medially, PTN THir somata were also scattered farther laterally (Fig 12a, b). Medial PTN THir somata lay primarily just dorsal to Hc, but a few cells also lay as far dorsal as the dorsal edge of LR (Fig 3c, d). PTN THir somata diameters were not significantly different (*t*-test; p-value = 0.35) between cave (mean diameter 8.0 ± 1.9 μm; N = 187) and surface *Astyanax* (mean diameter 7.8 ± 1.4 μm; N = 83; Fig 12c). PTN THir fibers projected laterally past Hc as well as dorsally, medial to THir fibers in the TGT. PTN THir fibers formed a dense column the width of Hc along the medial hypothalamus (Fig 3c, d). THir fibers were also evident in TS (Fig 3c, d).

Rhombencephalon

THir cells lay in the locus coeruleus (LC). These were magnocellular (< 40 μm), ellipsoid shaped somata ventral and lateral to the griseum centrale (GC; Fig 3g, h). LC THir somata were not numerous but were significantly larger in diameter (*t*-test; p-value < 0.001) in cave *Astyanax* (mean diameter 22.5 ± 5.6 μm; N = 68) than in surface *Astyanax* (mean diameter 19.1 ± 4.5 μm; N = 43; Fig 12f). The fibers from LC THir somata appeared sparse and thick and sent projections laterally and rostrocaudally, ventral to the THir somata (Fig 1 b, e; Fig 12d, e). THir somata rostral to LC are likely dopaminergic, whereas somata in the LC and further caudal are noradrenergic (Ma, 1997).

We also found THir fibers in the tectobulbar tracts (TTB, TTBc, TTBr; Fig 3e-h; Fig 4a, b) throughout the rhombencephalon and in the interpeduncular nucleus (IPN; Fig 3e, f), GC (Fig 3g, h; Fig 11 b, e; Fig 12d, e), the superior raphe (SR; Fig 3g, h), and the cerebellum (Fig 4). In the cave *Astyanax*, we found THir fibers in the secondary gustatory nucleus (SGN), that were not apparent in surface *Astyanax* (Fig 4 a, b). Finally, we found THir fibers in the magnocellular octaval nucleus (MON), the secondary octaval population (SO), the eight cranial nerve (VIII), and the secondary gustatory tract (SGT) as well as along the ventral edge of the rhombencephalon (Fig 4c-f).

Discussion

We characterized differences in TH immunoreactivity between surface (ancestral) and cave (derived) forms of *Astyanax*. THir somata in cave *Astyanax* had significantly larger diameters than surface *Astyanax* in the OB, MOT, PPa, PPp, SCN, VL, TPp, adjacent to PVO, and LC. The diameters of THir somata in Vi, VM, PPr, and PTN were not significantly between forms. THir fibers were found in each region with THir somata. THir fibers also appeared in TeO, PGl, LH, IL, Ts, TTB, IPN, SR, MON, VIII, and SGT. Importantly, we saw THir fibers in TGN and SGN in cave *Astyanax* but not surface fish.

Increases in the size of catecholaminergic neurons in cave *Astyanax* occurred in brain areas associated with non-visual sensory systems. Catecholaminergic modulation of these areas contributes to finding food in the absence of visual cues, the regulation of attention and locomotor activity, and energy homeostasis. It is likely that increases in the size of these neurons are correlated with increases in catecholaminergic signaling, which would result in changes in behavioral responsivity. Indeed, these findings are consistent with the hypothesis that adaptations to life in caves includes changes in behavioral control.

Generations before the emergence of the stereotypical suites of complex morphological adaptations to life in caves emerge, such as the loss of visual systems and pigmentation, animals may make behavioral changes that increase survival and reproduction in the absence of visual cues and a reduction or elimination of predation (Ghahramani et al., 2018). Changes to catecholaminergic systems, which affect the selection and strength of behavioral responses, may be a critical substrate for these sorts of behavioral modifications. For example, escape responses to unexpected sensory stimuli can be effective at reducing predation rates. However, escape responses are both energetically costly and incur

opportunity costs when feeding. Increases in catecholaminergic signaling may increase inhibition of unnecessary fear responses, thereby reducing energetic and opportunity costs.

Catecholamines in teleosts

The pattern of THir neuron staining in the *Astyanax* brain is consistent with reports in other teleost fishes. Conserved regions of THir include the olfactory bulb, basal telencephalon, preoptic, pretectal, tuberal, and rhombenclephalic areas (Ekström et al., 1990; Hornby & Piekut, 1990; Sas et al., 1990; Manso et al., 1993; Ma 1994a, 1994b, 1997, 2003; Meek & Joosten, 1993; Brinon et al., 1998; Rodnguez-Gomez et al., 2000; Rink & Wullimann, 2001; Filippi et al., 2009; Forlano et al., 2014; Goebrecht et al., 2014). For a review of THir reactivity in bony fishes see Meek (1994).

Catecholaminergic adaptation to life in caves

Brain regions in cave *Astyanax* with larger THir somata than their surface cousins are involved in the regulation of responses to behavioral cues that can affect survival in caves. For example, the olfactory and gustatory systems are sensory modalities that can be critical for life without visual cues (Menuet et al., 2007; Kasumyan et al., 2013; Espinasa et al., 2014; Hinaux et al., 2016). These chemosensory modalities are enhanced in cave *Astyanax* (Varatharasan et al., 2009; Yammamoto et al. 2009; Shiriagin & Korsching, 2018; Hinaux et al., 2016), and we show increased catecholaminergic innervation compared to the surface *Astyanax*.

In the olfactory system, we found larger THir somata in the OB and MOT. These areas also send olfactory information to Vv and Dp, which are reported to be homologues of the mammalian olfactory cortex and septal area, respectively (Rink & Wullimannn, 2004; Schärer et al., 2012). In the gustatory system (Wullimann, 1997; Rink & Wullimann, 1998; Folgueira et al., 2003), we found larger THir somata in PPp in cave *Astyanax*. We also observed THir fibers in the SGN and TGN that did not appear in surface *Astyanax*. In these systems, increases in catecholamine signaling may enhance chemosensory discrimination through lateral inhibition (Kermen et al., 2013).

We observed increased catecholaminergic innervation in brain areas that are involved in associative learning and motor control. Increases in THir in the OB may augment memory association to odorants through noradrenergic signaling (Ma, 1994b; Satou et al., 2006). Further, larger THir somata in the MOT in cave *Astyanax* may correspond to changes in the higher order processing in the forebrain (Von Bartheld et al., 1984). Increased catecholaminergic modulation of Dp has been shown to enhance odor memory (Schärer et al., 2012), while increased modulation of Vv mediates behavioral responses to particular odorants (Yaksi et al., 2009). Finally, increased inhibition of Vi, believed to be a homologue of the medial amygdala (Biechl et al., 2017), by larger TPp type 2 neurons in cavefish may both suppress escape behaviors to novel stimuli and increase exploratory behaviors via modulation of motor systems in the hindbrain (Scalia & Winans, 1975; Lehman et al., 1980; Fernandez-Fewell and Meredith, 1994; Canteras et al., 1995; McGregor et al., 2004; Choi et al., 2005; Brennan & Zufall, 2006; Tay et al., 2011; LeDoux, 2012; Keshavarz et al., 2014; Forlano et al., 2017).

In contrast, we did not observe differences in THir labeling in brain areas that are involved in the processing of visual information, except for VL and SCN. Despite the loss of vision in cave *Astyanax*, these fish nevertheless exhibit catecholaminergic modulation in visual nuclei (VM, PPr; Ekström, 1984; Northcutt & Wullimann, 1988; Northcutt & Butler, 1991). This result might be inhibitory (Perelmuter et al., 2019). However, catecholaminergic modulation of visual regions is more likely misleading, as the loss of THir staining due to reduced visual inputs may be offset by increased THir staining related to the modulation of other sensory modalities that are processed in the same brain areas, such as the TeO (Voneida & Fish, 1984). Consider VL, a visual nucleus (Ekström, 1984; Northcutt & Wullimann, 1988; Northcutt & Butler, 1991) in which we observed enlarged THir somata in cave *Astyanax*. VL also projects to the endohypothalamic tract, and we believe that the increase in the size of these cells may be related to changes in the regulation of endocrine release in the HPA axis (Tay et al., 2014). The larger diameter THir somata in SCN may decrease circadian activity cycles in cave *Astyanax* (Duboué et al., 2011; Beale et al., 2013).

Increased catecholamines in the brains of cave *Astyanax* may modulate stress responses through its effects on the HPA axis (Adinoff et al., 2005). For example, PPa activity, which has larger diameter THir somata in cavefish, inhibits endocrine release from the pituitary via DA signaling (Fontaine et al., 2015). Stress responses may also be reduced by activity in VL, Type 2 TPp, and PVO adjacent cells. Each of these areas sends projections to the endohypothalamic tract (Tay et al., 2014) and have larger THir neurons in cave *Astyanax*. These areas may inhibit, for example, corticotropin release. A decrease in corticotropin levels is associated with reduction of stress responses to predatory sensory signals, such as flight or freezing behaviors (Xu et al., 2019).

Acknowledgements

Abbreviations

Cant	Cant Anterior commissure
CC	Crista cerebellaris
CCe	Corpus cerebelli
CPN	Central pretectal nucleus
Cpost	Posterior commissure
Ctect	Tectal commissure
D	Dorsal telencephalon

Dl	Lateral zone of D
Dp	Posterior zone of D
DTN	Dorsal tegmental nucleus
ECL	External cell layer
EG	Eminentia granularis
GC	Griseum centrale
GL	Glomerular layer
Hc	Caudal zone of periventricular hypothalamus
Hd	Dorsal zone of periventricular hypothalamus
Hv	Ventral zone of periventricular hypothalamus
ICL	Internal cell layer
IL	Inferior lobe of hypothalamus
IPN	Interpeduncular nucleus
LC	Locus coeruleus
LFB	Lateral forebrain bundle
LH	Lateral hypothalamus
LOT	Lateral olfactory tract
LR	Lateral recess of the diencephalic ventricle
MFB	Median forebrain bundle
MON	Medial octavolateralis nucleus
MOT	Medial olfactory tract
PGl	Lateral preglomerular nucleus
PGZ	Periventricular gray zone of the optic tectum
PPa	Parvocellular preoptic nucleus
PPp	Posterior parvocellular preoptic nucleus
PPr	Periventricular pretectal nucleus
PR	Posterior recess of the diencephalic ventricle
PSm	Magnocellular superficial pretectal nucleus
PTN	Posterior tuberal nucleus

PVO	Paraventricular organ
RF	Reticular formation
SCN	Suprachiasmatic nucleus
SGN	Secondary gustatory nucleus
SGT	Secondary gustatory tract
SO	Secondary octaval population
SR	Superior raphe
TeO	Optic tectum
TeV	Tectal ventricle
TGN	Tertiary gustatory nucleus
TGT	Tertiary gustatory tract
TL	Torus longitudinalis
TPp	Periventricular nucleus of the posterior tuberculum
TS	Torus semicircularis
TTB	Tractus tectobulbaris
TTBc	Tractus tectobulbaris cruciatus
TTBr	Tractus tectobulbaris rectus
V	Ventral telencephalic area
Vd	Dorsal nucleus of V
Vi	Intermediate nucleus of V
VIII	Eighth cranial nerve
Vl	Lateral nucleus of V
VL	Ventrolateral thalamic nucleus
VM	Ventromedial thalamic nucleus
Vp	Postcommissural nucleus of V
VT	Ventral thalamic nuclei
Vv	Ventral nucleus of V

References:

Adinoff B, Junghanns K, Kiefer F, & Krishnan Sarin S (2005). Suppression of the HPA axis stress response: implications for relapse. Alcoholism: Clinical and Experimental Research, 29(7), 1351–1355.

Ahn S, & Phillips AG (2002). Modulation by central and basolateral amygdalar nuclei of dopaminergic correlates of feeding to satiety in the rat nucleus accumbens and medial prefrontal cortex. Journal of Neuroscience, 22(24), 10958–10965. [PubMed: 12486191]

Alioto TS, & Ngai J (2005). The odorant receptor repertoire of teleost fish. Bmc Genomics, 6(1), 173. [PubMed: 16332259]

Alonso JR, Covenas R, Lara J, Arevalo R, De Leon M, & Aijon J (1989). Tyrosine hydroxylase immunoreactivity in a subpopulation of granule cells in the olfactory bulb of teleost fish. Brain, behavior and evolution, 34(5), 318–324.

Aou S, Oomura Y, Nishino H, Inokuchi A, & Mizuno Y (1983). Influence of catecholamines on reward-related neuronal activity in monkey orbitofrontal cortex. Brain Research, 267(1), 165–170. [PubMed: 6860941]

Beale A, Guibal C, Tamai TK, Klotz L, Cowen S, Peyric E, … & Whitmore D (2013). Circadian rhythms in Mexican blind cavefish Astyanax mexicanus in the lab and in the field. Nature communications, 4, 2769.

Baeuml SW, Biechl D, & Wullimann MF (2019). Adult islet1 expression outlines ventralized derivatives along zebrafish neuraxis. Frontiers in neuroanatomy, 13.

Bibliowicz J, Alié A, Espinasa L, Yoshizawa M, Blin M, Hinaux H, … & Rétaux S(2013). Differences in chemosensory response between eyed and eyeless Astyanax mexicanus of the Rio Subterráneo cave. EvoDevo, 4(1), 25. [PubMed: 24007672]

Biechl D, Tietje K, Ryu S, Grothe B, Gerlach G, & Wullimannn MF (2017). Identification of accessory olfactory system and medial amygdala in the zebrafish. Scientific reports, 7, 44295. [PubMed: 28290515]

Björklund A, & Dunnett SB (2007). Fifty years of dopamine research. Trends in neurosciences, 30(5), 185–187. [PubMed: 17397938]

Boudriot F, & Reutter K (2001). Ultrastructure of the taste buds in the blind cave fish Astyanax jordani ("Anoptichthys") and the sighted river fish Astyanax mexicanus (Teleostei, Characidae). Journal of Comparative Neurology, 434(4), 428–444. [PubMed: 11343291]

Brinon JG, Arévalo R, Weruaga E, Crespo C, Alonso JR, & Aijon J (1998). Tyrosine hydroxylase-like immunoreactivity in the brain of the teleost fish Tinca tinca. Archives italiennes de biologie, 136(1), 17–44. [PubMed: 9492943]

Brown JS (1999). Vigilance, patch use and habitat selection: foraging under predation risk. Evolutionary ecology research, 1(1), 49–71.

Bundschuh ST, Zhu P, Schärer YPZ, & Friedrich RW (2012). Dopaminergic modulation of mitral cells and odor responses in the zebrafish olfactory bulb. Journal of Neuroscience, 32(20), 6830–6840. [PubMed: 22593052]

Calabresi P, Picconi B, Tozzi A, & Di Filippo M (2007). Dopamine-mediated regulation of corticostriatal synaptic plasticity. Trends in neurosciences, 30(5), 211–219. [PubMed: 17367873]

Candy J, & Collet C (2005). Two tyrosine hydroxylase genes in teleosts. Biochimica et Biophysica Acta (BBA)-Gene Structure and Expression, 1727(1), 35–44. [PubMed: 15652156]

Chakravarthy VS, Joseph D, & Bapi RS (2010). What do the basal ganglia do? A modeling perspective. Biological cybernetics, 103(3), 237–253. [PubMed: 20644953]

Deslauriers J, Toth M, Zhou X, & Risbrough V (2019). Heritable differences in catecholamine signaling modulate susceptibility to trauma and response to methylphenidate treatment: relevance for PTSD. Frontiers in behavioral neuroscience, 13, 111. [PubMed: 31164811]

Duboué ER, Borowsky RL, & Keene AC (2012). β-adrenergic signaling regulates evolutionarily derived sleep loss in the Mexican cavefish. Brain, behavior and evolution, 80(4), 233–243.

Duboué ER, Keene AC, & Borowsky RL (2011). Evolutionary convergence on sleep loss in cavefish populations. Current biology, 21(8), 671–676. [PubMed: 21474315]

Echteler SM (1985). Organization of central auditory pathways in a teleost fish, Cyprinus carpio. Journal of Comparative Physiology A, 156(2), 267–280.

Edwards JG, & Michel WC (2002). Odor-stimulated glutamatergic neurotransmission in the zebrafish olfactory bulb. Journal of Comparative Neurology, 454(3), 294–309. [PubMed: 12442320]

Ekström P (1984). Central neural connections of the pineal organ and retina in the teleost Gasterosteus aculeatus L. Journal of Comparative Neurology, 226(3), 321–335. [PubMed: 6747025]

Ekström P, Honkanen T, & Steinbusch HW (1990). Distribution of dopamine-immunoreactive neuronal perikarya and fibres in the brain of a teleost, Gasterosteus aculeatus L. comparison with tyrosine hydroxylase-and dopamine- beta-hydroxylase-immunoreactive neurons. Journal of chemical neuroanatomy, 3(4), 233–260. [PubMed: 1975745]

Elliott RE (2015). Cave biodiversity and ecology of the Sierra de El Abra region Biology and evolution of the Mexican cavefish. Elsevier, Amsterdam, 59–75.

Espinasa L, Bibliowicz J, Jeffery WR, & Rétaux S (2014). Enhanced prey capture skills in Astyanax cavefish larvae are independent from eye loss. EvoDevo, 5(1), 35. [PubMed: 25908953]

Fernandes CS, Batalha MA, & Bichuette ME (2016). Does the cave environment reduce functional diversity? PloS one, 11(3), e0151958. [PubMed: 27003837]

Folgueira M, Anadón R, & Yáñez J (2003). Experimental study of the connections of the gustatory system in the rainbow trout, Oncorhynchus mykiss. Journal of Comparative Neurology, 465(4), 604–619. [PubMed: 12975819]

Fontaine R, Affaticati P, Bureau C, Colin I, Demarque M, Dufour S, … & Pasqualini C (2015). Dopaminergic neurons controlling anterior pituitary functions: anatomy and ontogenesis in zebrafish. Endocrinology, 156(8), 2934–2948. [PubMed: 25965960]

Forlano PM, Kim SD, Krzyminska ZM, & Sisneros JA (2014). Catecholaminergic connectivity to the inner ear, central auditory, and vocal motor circuitry in the plainfin midshipman fish Porichthys notatus. Journal of Comparative Neurology, 522(13), 2887–2927. [PubMed: 24715479]

Forlano PM, Licorish RR, Ghahramani ZN, Timothy M, Ferrari M, Palmer WC, & Sisneros JA (2017). Attention and motivated response to simulated male advertisement call activates forebrain dopaminergic and social decision-making network nuclei in female midshipman fish. Integrative and comparative biology, 57(4), 820–834. [PubMed: 28992072]

Fumey J, Hinaux H, Noirot C, Thermes C, Rétaux S, & Casane D (2018). Evidence for late Pleistocene origin of Astyanax mexicanus cavefish. BMC evolutionary biology, 18(1), 43. [PubMed: 29665771]

Fuller CL, Yettaw HK, & Byrd CA (2006). Mitral cells in the olfactory bulb of adult zebrafish (Danio rerio): morphology and distribution. Journal of Comparative Neurology, 499(2), 218–230. [PubMed: 16977629]

Gertychowa R (1970). Studies on the ethology and space orientation of the blind cave fish Anoptichthys jordani Hubbs et Innes 1936 (Characidae). Folia biologica, 18(1), 9. [PubMed: 5433416]

Gordon MS (1958). The Physiology of the Pituitary Gland of Fishes. Copeia, 1958(1), 61–62.

Ghahramani ZN, Timothy M, Varughese J, Sisneros JA, & Forlano PM (2018). Dopaminergic neurons are preferentially responsive to advertisement calls and co-active with social behavior network nuclei in sneaker male midshipman fish. Brain research, 1701, 177–188. [PubMed: 30217439]

Grunewald-Lowenstein M (1956). Influence of light and darkness on the pineal body in Astyanax mexicanus (Filippi). Zoologica, 41, 119–128.

Gillespie RG, & Caraco T (1987). Risk-sensitive foraging strategies of two spider populations. Ecology, 68(4), 887–899.

Hajnal A, & Norgren R (2005). Taste pathways that mediate accumbens dopamine release by sapid sucrose. Physiology & behavior, 84(3), 363–369. [PubMed: 15763573]

Hinaux H, Devos L, Blin M, Elipot Y, Bibliowicz J, Alié A, & Rétaux S (2016). Sensory evolution in blind cavefish is driven by early embryonic events during gastrulation and neurulation. Development, 143(23), 4521–4532. [PubMed: 27899509]

Hinaux H, Rétaux S, & Elipot Y (2015). Social Behavior and Aggressiveness in Astyanax.

Honkanen T, & Ekström P (1990). An immunocytochemical study of the olfactory projections in the three-spined stickleback, Gasterosteus aculeatus, L. Journal of Comparative Neurology, 292(1), 65–72. [PubMed: 1968916]

Hornby PJ, & Piekut DT (1990). Distribution of catecholamine-synthesizing enzymes in goldfish brains: presumptive dopamine and norepinephrine neuronal organization. Brain, behavior and evolution, 35(1), 49–64.

Howarth FG (1993). High-stress subterranean habitats and evolutionary change in cave-inhabiting arthropods. The American Naturalist, 142, S65–S77.

Jaggard J, Robinson BG, Stahl BA, Oh I, Masek P, Yoshizawa M, & Keene AC (2017). The lateral line confers evolutionarily derived sleep loss in the Mexican cavefish. Journal of Experimental Biology, 220(2), 284–293. [PubMed: 28100806]

Jeffery WR (2005). Adaptive evolution of eye degeneration in the Mexican blind cavefish. Journal of Heredity, 96(3), 185–196. [PubMed: 15653557]

Kasumyan AO, & Marusov EA (2015). Chemoorientation in the feeding behavior of the blind Mexican cavefish Astyanax fasciatus (Characidae, Teleostei). Russian journal of ecology, 46(6), 559–563.

Kasumyan AO, & Marusov EA (2018). Odor Stimulation and Relation to Taste Stimuli in the Blind Cave Fish Astyanax fasciatus. Biology Bulletin, 45(6), 557–563.

Katz DB, & Sadacca BF (2011). 6 Taste. Neurobiology of Sensation and Reward, 127.

Keene A, Yoshizawa M, & McGaugh SE (2015). Biology and evolution of the Mexican cavefish. Academic Press.

Kermen F, Franco LM, Wyatt C, & Yaksi E (2013). Neural circuits mediating olfactory-driven behavior in fish. Frontiers in neural circuits, 7, 62. [PubMed: 23596397]

Keshavarzi S, Sullivan RK, Ianno DJ, & Sah P (2014). Functional properties and projections of neurons in the medial amygdala. Journal of Neuroscience, 34(26), 8699–8715. [PubMed: 24966371]

Kiyokage E, Pan YZ, Shao Z, Kobayashi K, Szabo G, Yanagawa Y, … & Shipley MT (2010). Molecular identity of periglomerular and short axon cells. Journal of Neuroscience, 30(3), 1185–1196. [PubMed: 20089927]

Kosaka K, & Kosaka T (2005). Synaptic organization of the glomerulus in the main olfactory bulb: compartments of the glomerulus and heterogeneity of the periglomerular cells. Anatomical science international, 80(2), 80–90. [PubMed: 15960313]

Kosaka T, & Kosaka K (2011). "Interneurons" in the olfactory bulb revisited. Neuroscience research, 69(2), 93–99. [PubMed: 20955739]

Ma PM (1994). Catecholaminergic systems in the zebrafish. I. Number, morphology, and histochemical characteristics of neurons in the locus coeruleus. Journal of Comparative Neurology, 344(2), 242–255. [PubMed: 8077459]

Ma PM (1994). Catecholaminergic systems in the zebrafish. II. Projection pathways and pattern of termination of the locus coeruleus. Journal of Comparative Neurology, 344(2), 256–269. [PubMed: 8077460]

Ma PM (1997). Catecholaminergic systems in the zebrafish. III. Organization and projection pattern of medullary dopaminergic and noradrenergic neurons. Journal of Comparative Neurology, 381(4), 411–427. [PubMed: 9136799]

Ma PM (2003). Catecholaminergic systems in the zebrafish. IV. Organization and projection pattern of dopaminergic neurons in the diencephalon. Journal of Comparative Neurology, 460(1), 13–37. [PubMed: 12687694]

Manso MJ, Becerra M, Molist P, Rodriguez-Moldes I, & Anadón R (1993). Distribution and development of catecholaminergic neurons in the brain of the brown trout. A tyrosine hydroxylase immunohistochemical study. Journal fur Hirnforschung, 34(2), 239–260. [PubMed: 7901271]

Meek J, & Joosten HWJ (1993). Tyrosine hydroxylase-immunoreactive cell groups in the brain of the teleost fish Gnathonemus petersii. Journal of chemical neuroanatomy, 6(6), 431–446. [PubMed: 7908204]

Meek J (1994). Catecholamines in the brains of Osteichthyes (bony fishes). Phylogeny and Development of Catecholamine Systems in the CNS of Vertebrates, 49–76.

Mendoza J, & Challet E (2014). Circadian insights into dopamine mechanisms. Neuroscience, 282, 230–242. [PubMed: 25281877]

Menuet A, Alunni A, Joly JS, Jeffery WR, & Rétaux S (2007). Expanded expression of Sonic Hedgehog in Astyanax cavefish: multiple consequences on forebrain development and evolution. Development, 134(5), 845–855. [PubMed: 17251267]

Miyasaka N, Morimoto K, Tsubokawa T, Higashijima SI, Okamoto H, & Yoshihara Y (2009). From the olfactory bulb to higher brain centers: genetic visualization of secondary olfactory pathways in zebrafish. Journal of Neuroscience, 29(15), 4756–4767. [PubMed: 19369545]

Moore P, & Crimaldi J (2004). Odor landscapes and animal behavior: tracking odor plumes in different physical worlds. Journal of marine systems, 49(1-4), 55–64.

Nakano Y, Lenard L, Oomura Y, Nishino H, Aou S, & Yamamoto T (1987). Functional involvement of catecholamines in reward-related neuronal activity of the monkey amygdala. Journal of neurophysiology, 57(1), 72–91. [PubMed: 3559682]

Northcutt RG, & Butler AB (1991). Retinofugal and Retinopetal Projections in the Green Sunfish, Lepomis cyanellus (Part 1 of 2). Brain, behavior and evolution, 37(6), 333–343.

Northcutt RG, & Wullimann MF (1988). The visual system in teleost fishes: morphological patterns and trends In Sensory biology of aquatic animals (pp. 515–552). Springer, New York, NY.

Olivares J, & Schmachtenberg O (2019). An update on anatomy and function of the teleost olfactory system. PeerJ, 7, e7808. [PubMed: 31579633]

Park J, Wheeler RA, Fontillas K, Keithley RB, Carelli RM, & Wightman RM (2012). Catecholamines in the bed nucleus of the stria terminalis reciprocally respond to reward and aversion. Biological psychiatry, 71(4), 327–334. [PubMed: 22115620]

Perelmuter JT, Wilson AB, Sisneros JA, & Forlano PM (2019). Forebrain dopamine system regulates inner ear auditory sensitivity to socially relevant acoustic signals. Current Biology, 29(13), 2190–2198. [PubMed: 31204161]

Pfeiffer W (1966). Über die Vererbung der Schreckreaktion beiAstyanax (Characidae, Pisces). Molecular and General Genetics MGG, 98(2), 97–105.

Poschel BPH, & Ninteman FW (1963). Norepinephrine: a possible excitatory neurohormone of the reward system. Life sciences, 2(10), 782–788.

Prokopova I (2010). Noradrenaline and behavior. Ceskoslovenská fysiologie, 59(2), 51–58. [PubMed: 21254660]

Protas M, Tabansky I, Conrad M, Gross JB, Vidal O, Tabin CJ, & Borowsky R (2008). Multi-trait evolution in a cave fish, Astyanax mexicanus. Evolution & development, 10(2), 196–209. [PubMed: 18315813]

Purves D, Augustine GJ, Fitzpatrick D, Hall WC, LaMantia AS, McNamara JO, & White LE (2014). Neuroscience, 2008 De Boeck, Sinauer, Sunderland, Mass.

R Core Team (2017). R: A language and environment for statistical computing R Foundation for Statistical Computing, Vienna, Austria URL https://www.R-project.org/.

Rea P (2015). Essential clinical anatomy of the nervous system. Academic Press.

Rétaux S, Alié A, Blin M, Devos L, Elipot Y, & Hinaux H (2015). Neural development and evolution in Astyanax mexicanus: comparing cavefish and surface fish brains Biology of the Mexican Cavefish. San Diego, CA: Elsevier, 227–241.

Rincón L, Obando MJ, Tovar MO, Pandolfi M, & Hurtado H (2017). Topological and histological description of preoptic area and hypothalamus in cardinal tetra Paracheirodon axelrodi (Characiformes: Characidae). Neotropical Ichthyology, 15(1).

Rink E, & Wullimann MF (1998). Some forebrain connections of the gustatory system in the goldfish Carassius auratus visualized by separate DiI application to the hypothalamic inferior lobe and the torus lateralis. Journal of Comparative Neurology, 394(2), 152–170. [PubMed: 9552123]

Rink E, & Wullimann MF (2001). The teleostean (zebrafish) dopaminergic system ascending to the subpallium (striatum) is located in the basal diencephalon (posterior tuberculum). Brain research, 889(1-2), 316–330. [PubMed: 11166725]

Rink E, & Wullimann MF (2002). Connections of the ventral telencephalon and tyrosine hydroxylase distribution in the zebrafish brain (Danio rerio) lead to identification of an ascending dopaminergic system in a teleost. Brain research bulletin, 57(3-4), 385–387. [PubMed: 11922994]

Rink E, & Wullimann MF (2004). Connections of the ventral telencephalon (subpallium) in the zebrafish (Danio rerio). Brain research, 1011(2), 206–220. [PubMed: 15157807]

Rodríguez-Gomez FJ, Rendon-Unceta MC, Sarasquete C, & Muñoz-Cueto JA (2000). Localization of tyrosine hydroxylase-immunoreactivity in the brain of the Senegalese sole, Solea senegalensis. Journal of chemical neuroanatomy, 19(1), 17–32. [PubMed: 10882834]

Romero A, Green SM, Romero A, Lelonek MM, & Stropnicky KC (2003). One eye but no vision: cave fish with induced eyes do not respond to light. Journal of Experimental Zoology Part B: Molecular and Developmental Evolution, 300(1), 72–79.

Rosen JB (2017). Aversive emotions: Molecular basis of unconditioned fear.

Salin K, Voituron Y, Mourin J, & Hervant F (2010). Cave colonization without fasting capacities: an example with the fish Astyanax fasciatus mexicanus. Comparative Biochemistry and Physiology Part A: Molecular & Integrative Physiology, 156(4), 451–457.

Sas E, Maler L, & Tinner B (1990). Catecholaminergic systems in the brain of a gymnotiform teleost fish: an immunohistochemical study. Journal of Comparative Neurology, 292(1), 127–162. [PubMed: 1968915]

Saper CB, Scammell TE, & Lu J (2005). Hypothalamic regulation of sleep and circadian rhythms. Nature, 437(7063), 1257. [PubMed: 16251950]

Satou M, Hoshikawa R, Sato Y, & Okawa K (2006). An in vitro study of long-term potentiation in the carp (Cyprinus carpio L.) olfactory bulb. Journal of Comparative Physiology A, 192(2), 135–150.

Schärer YP, Shum J, Moressis A, & Friedrich RW (2012). Dopaminergic modulation of synaptic transmission and neuronal activity patterns in the zebrafish homolog of olfactory cortex. Frontiers in Neural Circuits, 6, 76. [PubMed: 23109918]

Schemmel C (1980). Studies on the genetics of feeding behaviour in the cave fish Astyanax mexicanus f. Anoptichthys: an example of apparent monofactorial inheritance by polygenes. Zeitschrift für Tierpsychologie, 53(1), 9–22. [PubMed: 7434991]

Schjolden J, Schiöth HB, Larhammar D, Winberg S, & Larson ET (2009). Melanocortin peptides affect the motivation to feed in rainbow trout (Oncorhynchus mykiss). General and comparative endocrinology, 160(2), 134–138. [PubMed: 19027741]

Schultz W (1998). Predictive reward signal of dopamine neurons. Journal of neurophysiology, 80(1), 1–27. [PubMed: 9658025]

Scotto-Lomassese S, Strambi C, Strambi A, Aouane A, Augier R, Rougon G, & Cayre M (2003). Suppression of adult neurogenesis impairs olfactory learning and memory in an adult insect. Journal of Neuroscience, 23(28), 9289–9296. [PubMed: 14561855]

Shiriagin V, & Korsching SI (2018). Massive expansion of bitter taste receptors in blind cavefish, Astyanax mexicanus. Chemical senses, 44(1), 23–32.

Sligar CM, & Voneida TJ (1976). Tectal efferents in the blind cave fish Astyanax hubbsi. Journal of Comparative Neurology, 165(1), 107–124. [PubMed: 1244359]

Strickler AG, & Soares D (2011). Comparative genetics of the central nervous system in epigean and hypogean Astyanax mexicanus. Genetica, 139(3), 383–391. [PubMed: 21318738]

Soares D, Yamamoto Y, Strickler AG, & Jeffery WR (2004). The lens has a specific influence on optic nerve and tectum development in the blind cavefish Astyanax. Developmental neuroscience, 26(5-6), 308–317. [PubMed: 15855759]

Varatharasan N, Croll RP, & Franz-Odendaal T (2009). Taste bud development and patterning in sighted and blind morphs of Astyanax mexicanus. Developmental Dynamics, 238(12), 3056–3064. [PubMed: 19877280]

Von Bartheld CS, Meyer DL, Fiebig E, & Ebbesson SOE (1984). Central connections of the olfactory bulb in the goldfish, Carassius auratus. Cell and tissue research, 238(3), 475–487. [PubMed: 6084554]

Voneida TJ, & Fish SE (1984). Central nervous system changes related to the reduction of visual input in a naturally blind fish (Astyanax hubbsi). American zoologist, 24(3), 775–782.

Wilkens H, & Hüppop K (1986). Sympatric speciation in cave fishes? Studies on a mixed population of epi-and hypogean Astyanax (Characidae, Pisces). Journal of Zoological Systematics and Evolutionary Research, 24(3), 223–230.

Wickham H (2016). ggplot2: Elegant Graphics for Data Analysis. Springer-Verlag, New York.

Wullimannn MF (1998). The central nervous system. The physiology of fishes, 245–282.

Yaksi E, von Saint Paul F, Niessing J, Bundschuh ST, & Friedrich RW (2009). Transformation of odor representations in target areas of the olfactory bulb. Nature neuroscience, 12(4), 474. [PubMed: 19305401]

Yamamoto Y, Byerly MS, Jackman WR, & Jeffery WR (2009). Pleiotropic functions of embryonic sonic hedgehog expression link jaw and taste bud amplification with eye loss during cavefish evolution. Developmental biology, 330(1), 200–211. [PubMed: 19285488]

Yoshizawa M, Gori ki Š, Soares D, & Jeffery WR (2010). Evolution of a behavioral shift mediated by superficial neuromasts helps cavefish find food in darkness. Current Biology, 20(18), 1631–1636. [PubMed: 20705469]

Yoshizawa M, Yamamoto Y, O'Quin KE, & Jeffery WR (2012). Evolution of an adaptive behavior and its sensory receptors promotes eye regression in blind cavefish. BMC biology, 10(1), 108. [PubMed: 23270452]

Xu JJ, Fu SJ, & Fu C (2019). Physiological and behavioral stress responses to predators are altered by prior predator experience in juvenile qingbo (Spinibarbus sinensis). Biology open, 8(5), bio041012. [PubMed: 31097443]
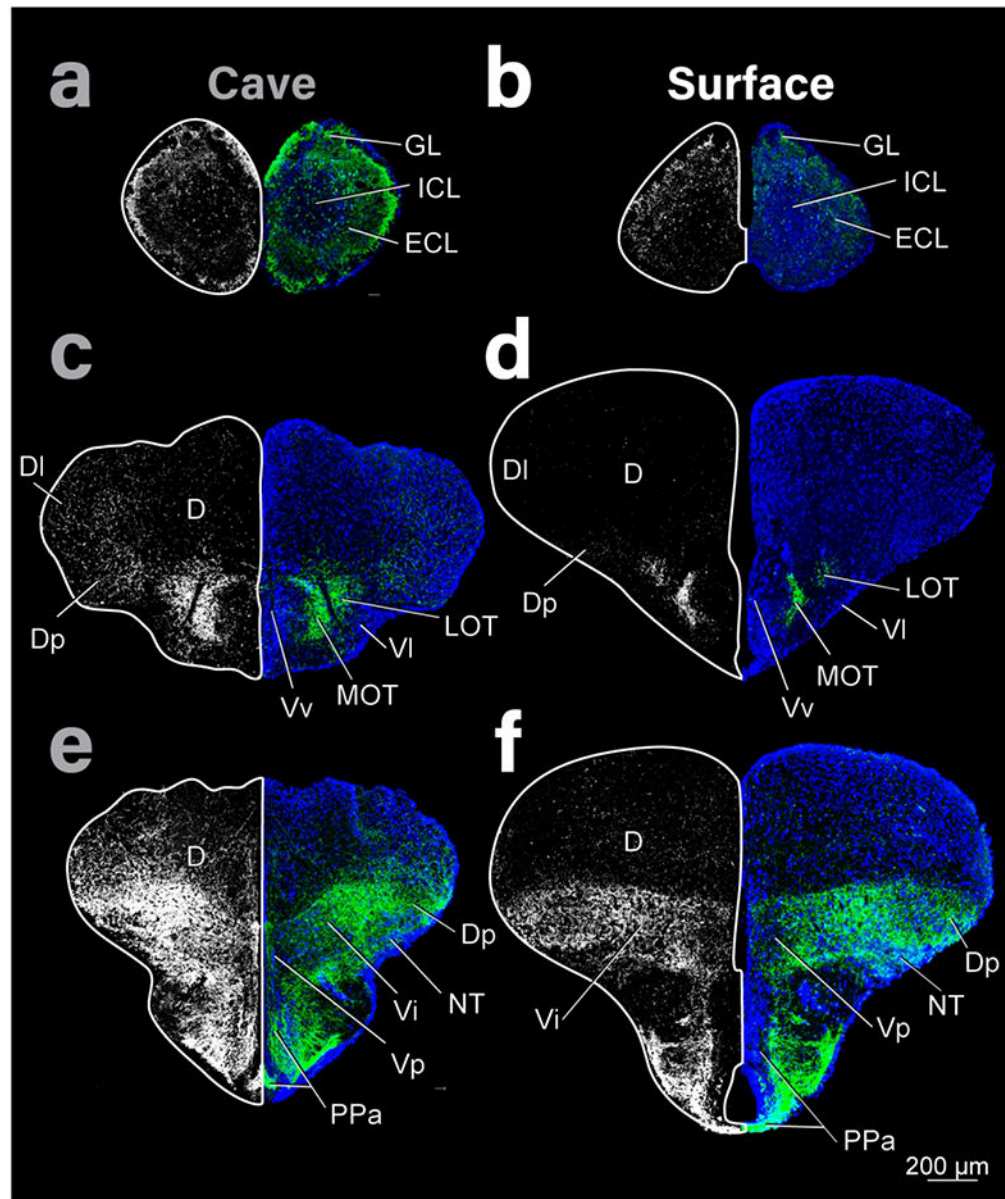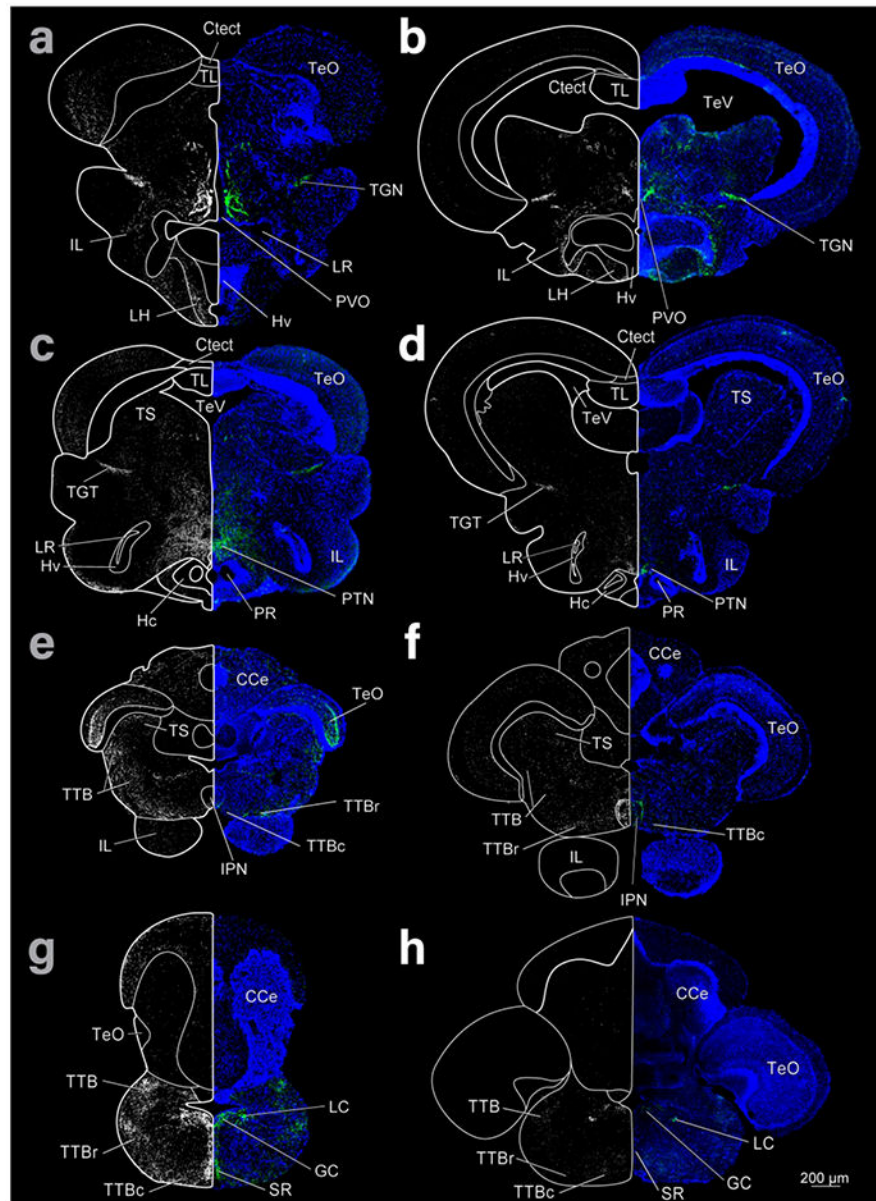
Figure 1:
Coronal sections of the telencephalon of cave (left column) and surface (right column) Astyanax showing THir staining (right and left hemispheres) and DAPI (blue, r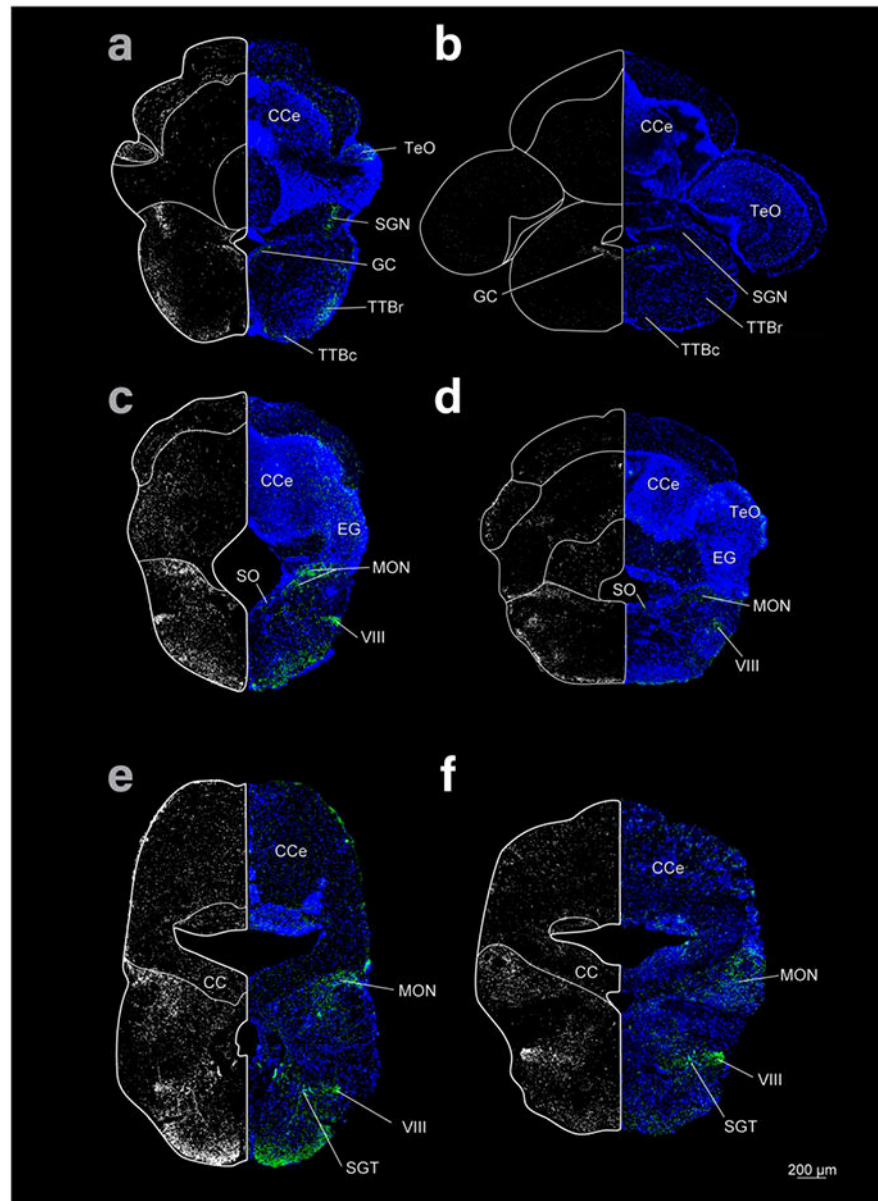ight hemisphere). Top row is most rostral and bottom caudal. THir images on both sides were generated from the same original image but shown in high contrast on the left to emphasize the distribution of immunoreactivity (see Methods for more details).
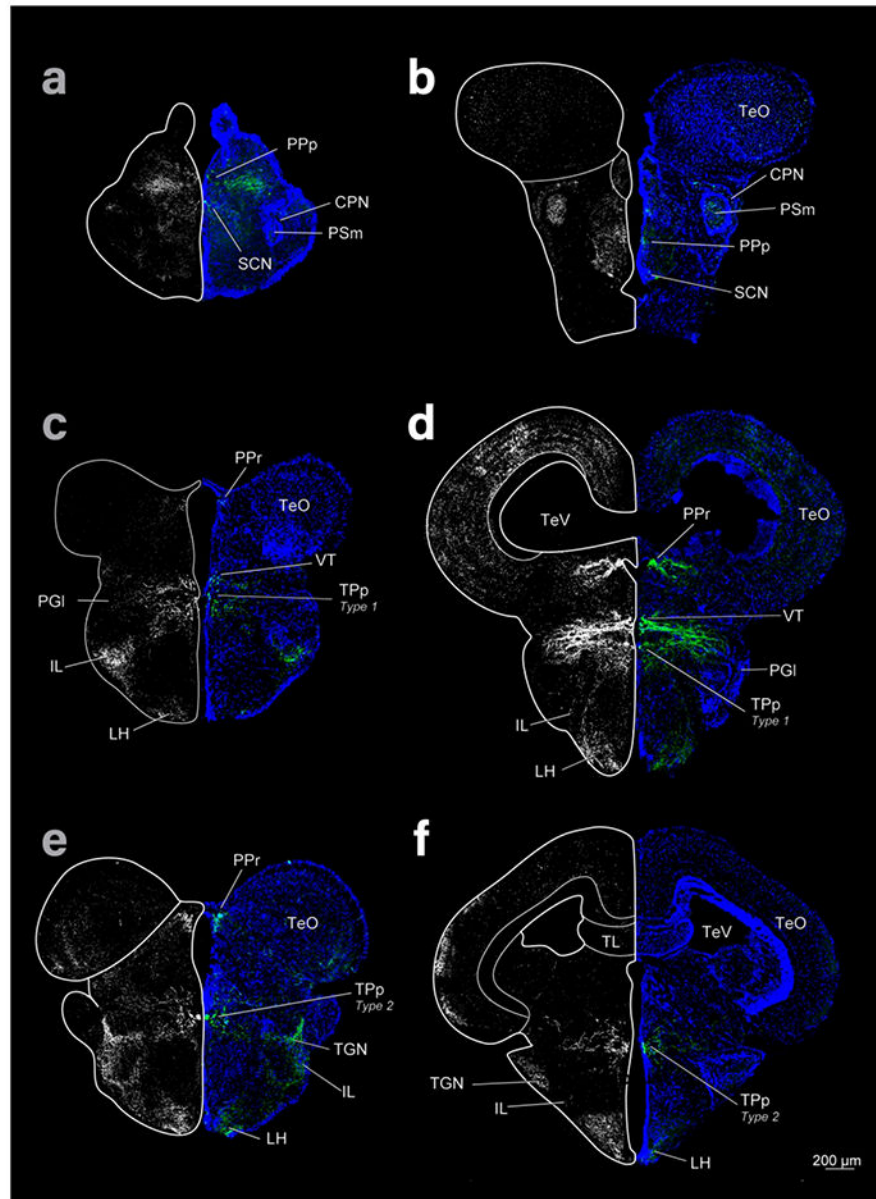
Figure 2:
Diencephalon and mesencephalon of cave (left column) and surface (right column) Astyanax showing THir labeling (grayscale images and green) and DAPI (blue) in coronal sections. Top row is rostral, bottom caudal.

Figure 3:
Coronal sections of cave (left column) and surface (right column) Astyanax showing THir staining (right and left hemispheres) and DAPI (blue, right hemisphere). Top row is most rostral and bottom caudal.

Figure 4:
Coronal sections of the rhombencephalon of cave (left column) and surface (right column) Astyanax showing THir staining (right and left hemispheres) and DAPI (blue, right hemisphere). Top row is most rostral and bottom caudal.
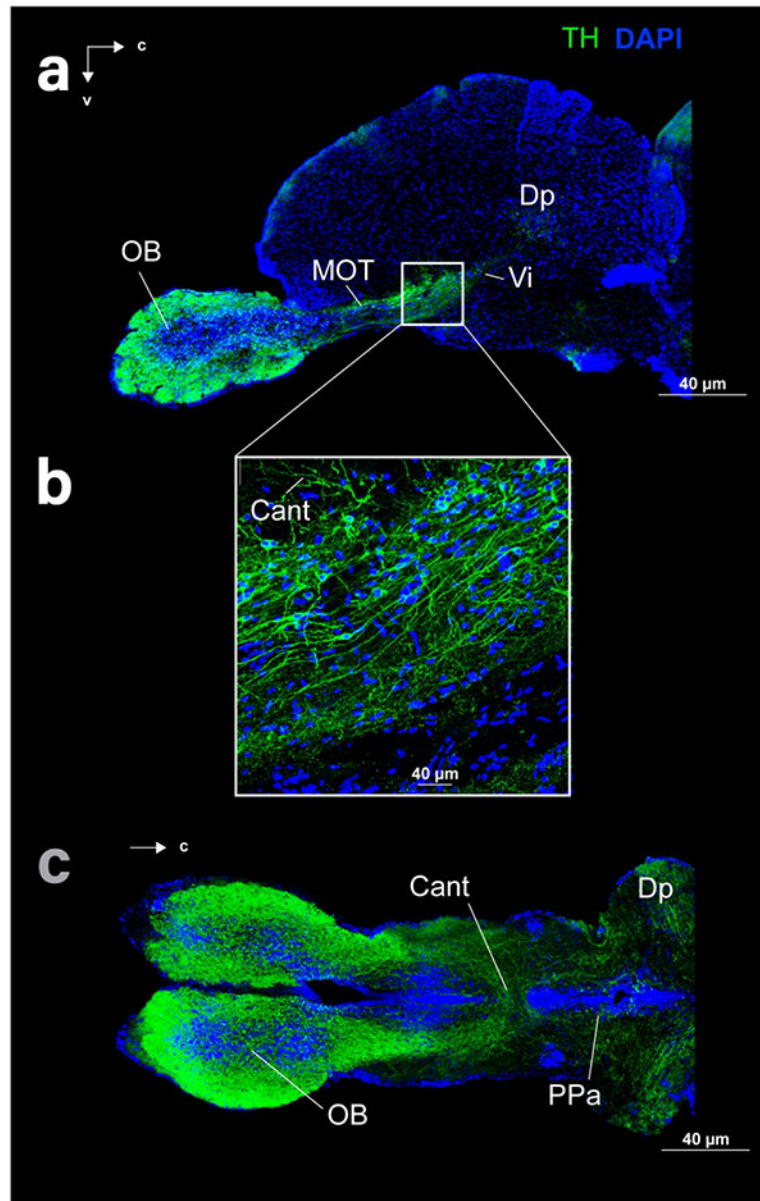
Figure 5:
Sagittal (a, b) and horizontal (c) sections of the telencephalon of cave (c) and surface (a, b) Astyanax showing THir (green) and DAPI (blue) staining.
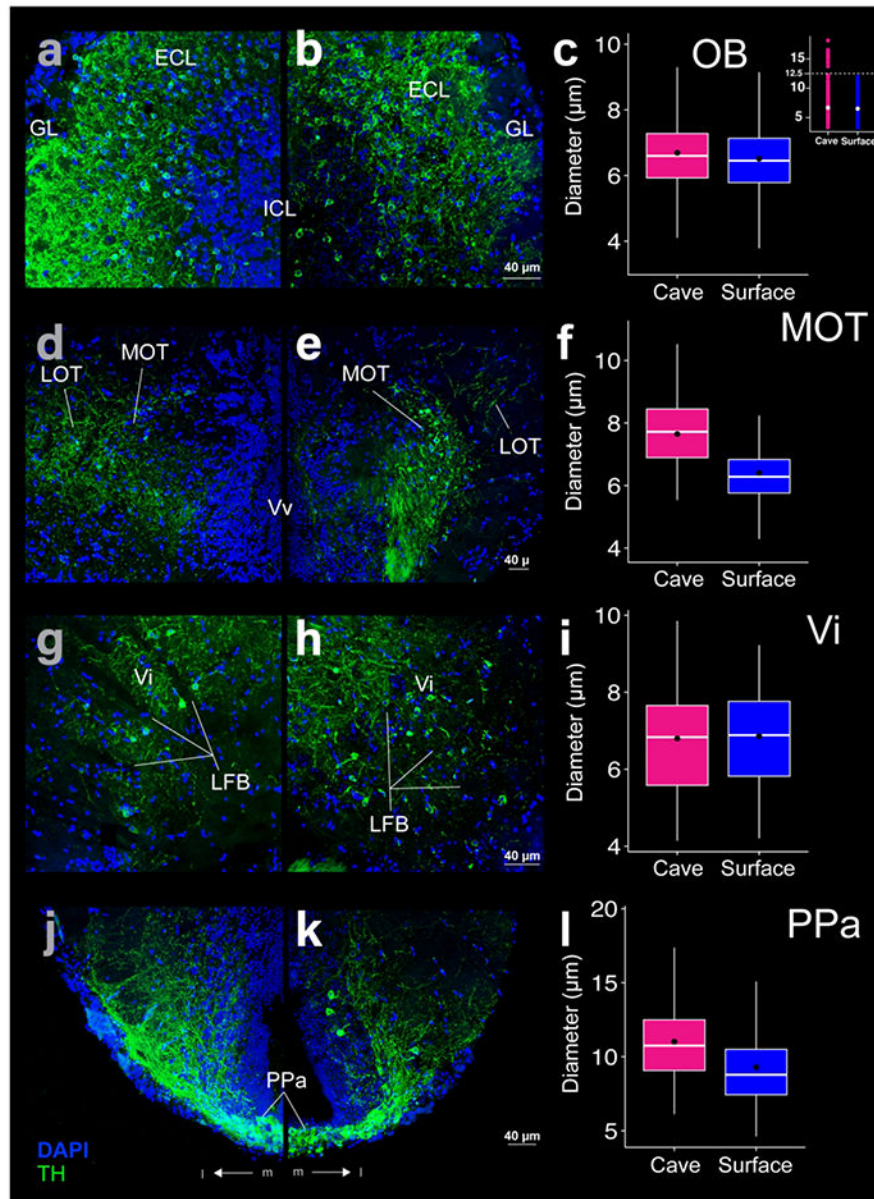
Figure 6:

THir (green) and DAPI (blue) stained coronal sections of cave (left; a, d ,g, j) and surface (right; b, e, h, k) Astyanax. THir labeled somata had significantly larger (p-value < 0.001) diameters in cave Astyanax than in surface Astyanax in the olfactory bulb (OB; a-c), medial olfactory tract (MOT; d-f), and anterior parvocellular preoptic nucleus (PPa; j-k) but not in the intermediate nucleus of the ventral telencephalic area (Vi; g-i). The box plots in the right column (c, f, i, l) show the distributions of THir somata diameters of cave (pink) and surface (blue) Astyanax for that row. Black dots are the mean diameter, middle white line is the median, limits of the colored box indicate quartiles, and vertical white lines extend to the minimum and maximum diameters. The inset in (c) shows the distribution of OB THir somata diameters of cave (pink) and surface (blue) Astyanax. Dotted line is the threshold for separation of two populations of neurons in cavefish.
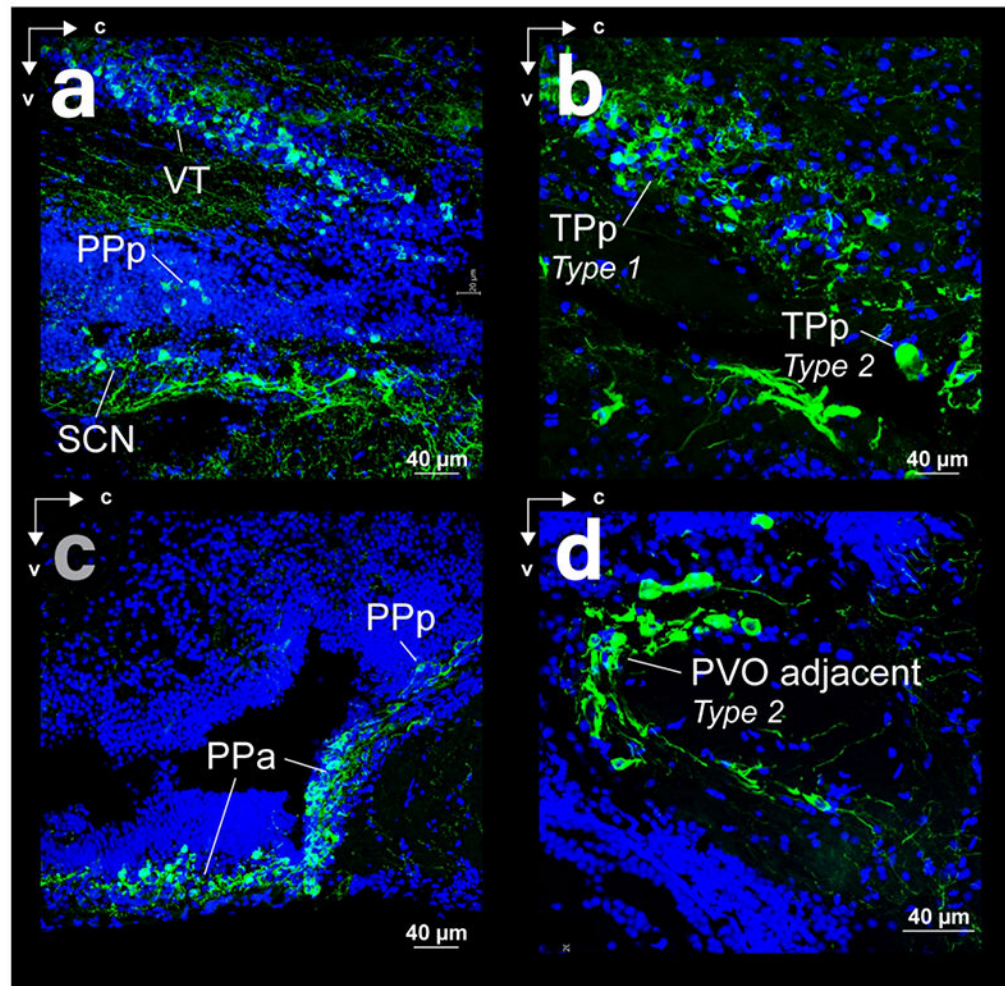
FFigure 7:
Spatial relations of somata and fibers in sagittal sections with THir (green) and DAPI (blue) staining. (a) Ventral thalamus (VT) and preoptic area of surface Astyanax (posterior parvocellular preoptic nucleus - PPp and suprachiasmatic nucleus - SCN). (b) Periventricular nucleus of the posterior tuberculum of surface Astyanax. (c) Anterior (PPa) and posterior (PPp) regions of the parvocellular reoptic nucleus of cave Astyanax. (d) Magnocellular type 2 neurons of the posterior tuberculum, adjacent to the periventricular ventral organ (PVO) of surface Astyanax.
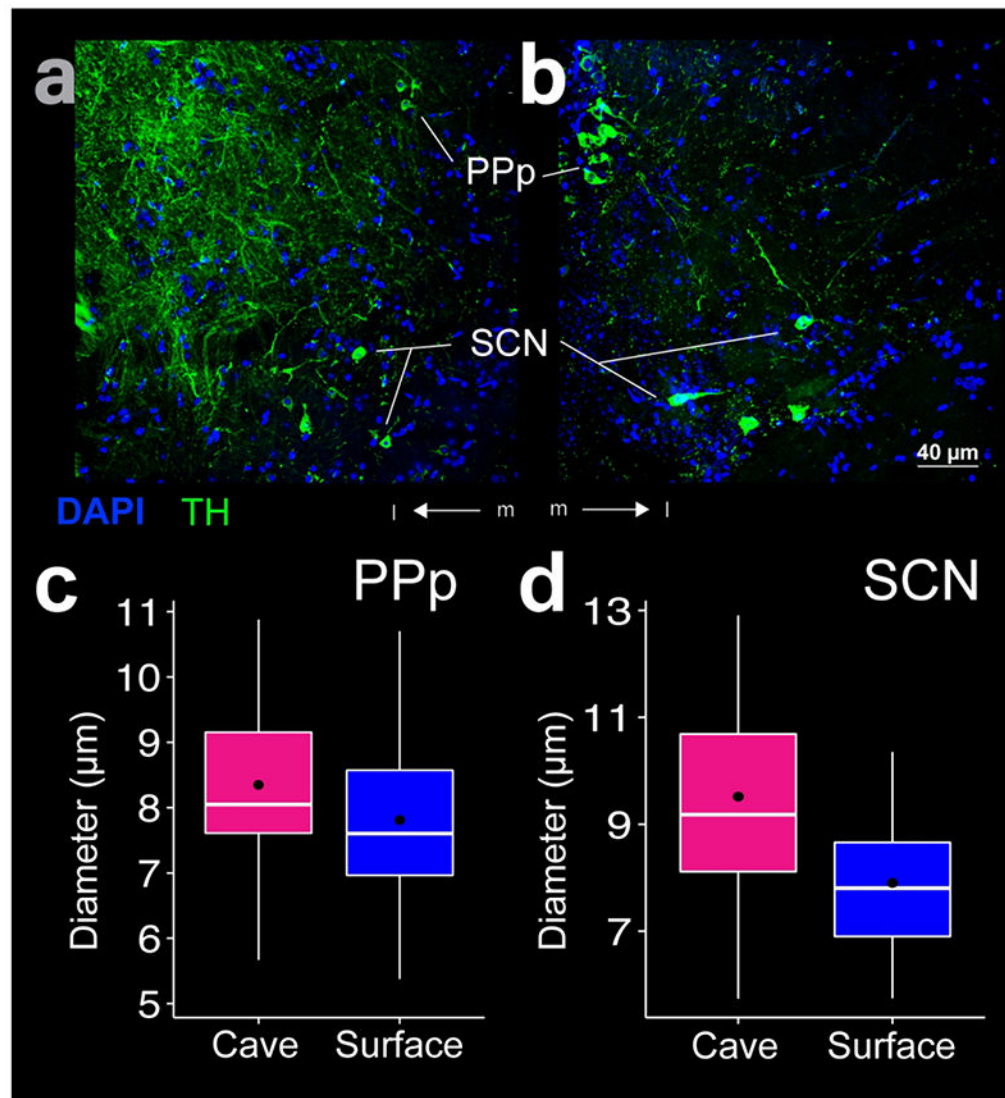
Figure 8:
THir labeling in the posterior parvocellular preoptic nucleus (PPp) and suprachiasmatic nucleus (SCN). Images of cave (a) and surface (b) Astyanax show THir (green) and DAPI (blue) immunoreactivity. The box plots (c, d) show that diameters of the THir somata were significantly larger (p < 0.01) in the cave form in both PPp (c) and SCN (d). Black dots are the mean diameter, middle white line is the median, limits of the colored box indicate quartiles, and vertical white lines extend to the minimum and maximum diameters.
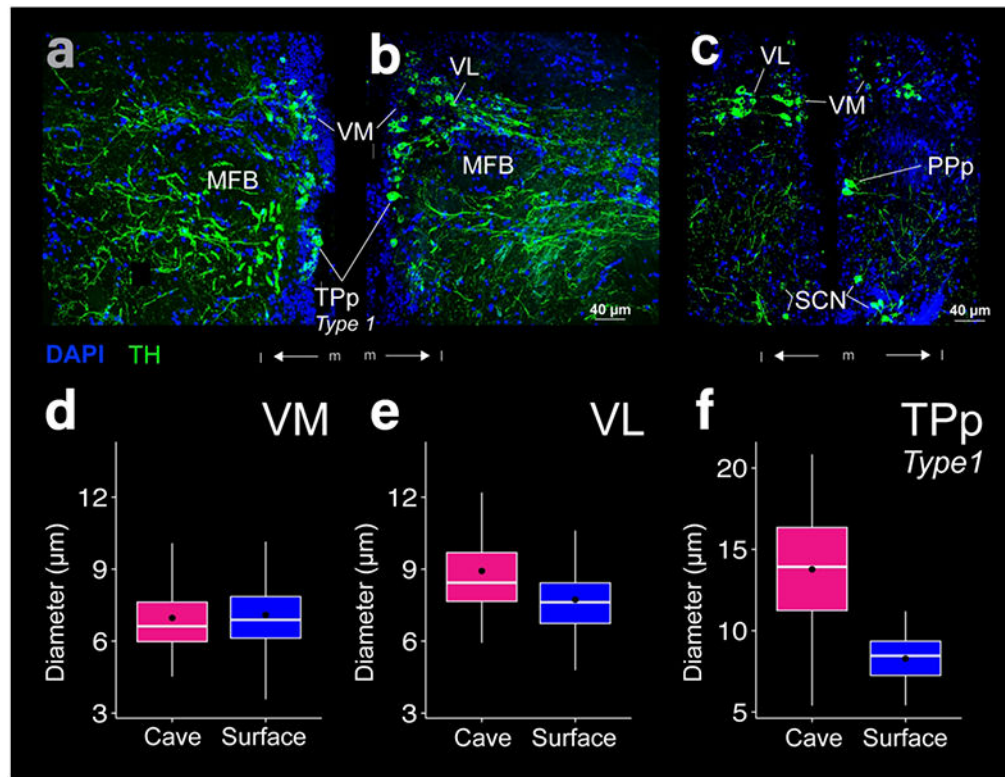
Figure 9:
THir labeling in the ventromedial thalamic nucleus (VM), ventrolateral thalamic nucleus (VL), and type 1 neurons of the periventricular nucleus of the posterior tuberculum (TPp). Images of cave (a) and surface (b, c) Astyanax show THir (green) and DAPI (blue) immunoreactivity. The box plots (d-f) show THir somata distributions that were significantly larger (p < 0.001) in the cave form in both VL and TPp type 1 neurons, but not in VM. Black dots are the mean diameter, middle white line is the median, limits of the colored box indicate quartiles, and vertical white lines extend to the minimum and maximum diameters.
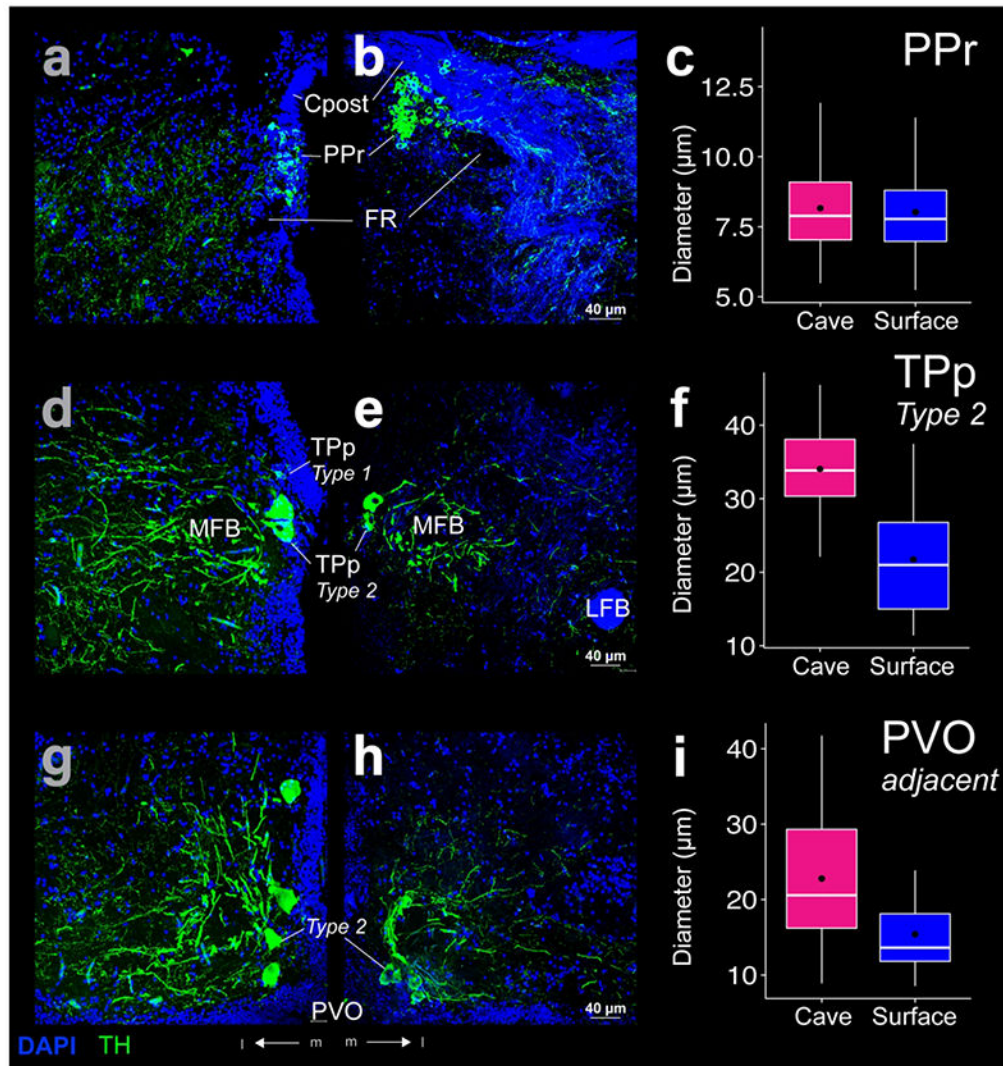
Figure 10:
THir (green) and DAPI (blue) stained coronal sections of cave (left; a, d, g) and surface (right; b, e, h) Astyanax. THir labeled somata had significantly larger (p < 0.001) diameters in cave Astyanax in the magnocellular pear shaped (type 2) cells of the periventricular nucleus of the posterior tuberculum (TPp; d-f) and adjacent to the paraventricular organ (PVO; g-i), but not in the periventricular pretectal nucleus (PPr; a-c). The box plots in the right column (c, f, i) show the distributions of THir somata diameters of cave (pink) and surface (blue) Astyanax for that row. Black dots are the mean diameter, middle white line is the median, limits of the colored box indicate quartiles, and vertical white lines extend to the minimum and maximum diameters.
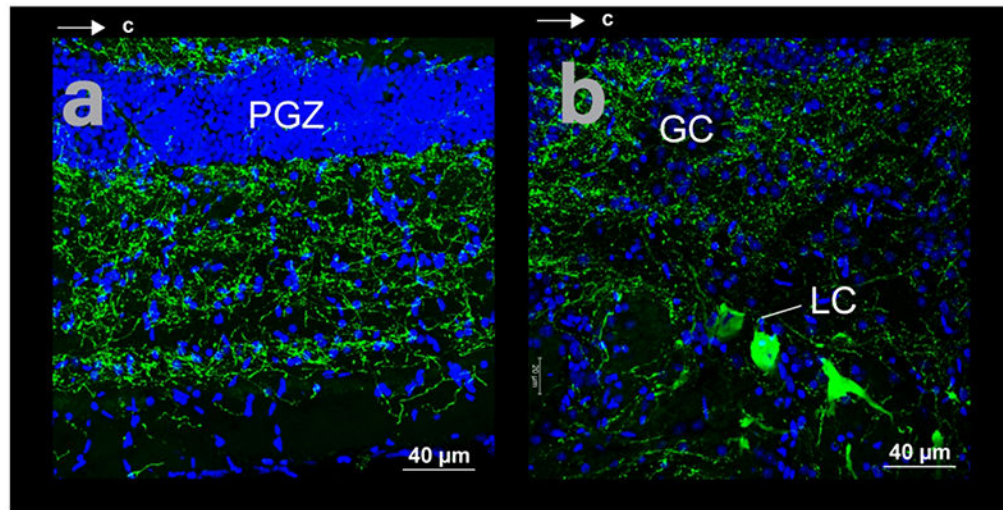
Figure 11:
Spatial relations of somata and fibers in horizontal sections with THir (green) and DAPI (blue) staining in cave Astyanax. (a) Optic tectum. (b) Locus coeruleus (LC) and griseum centrale (GC).
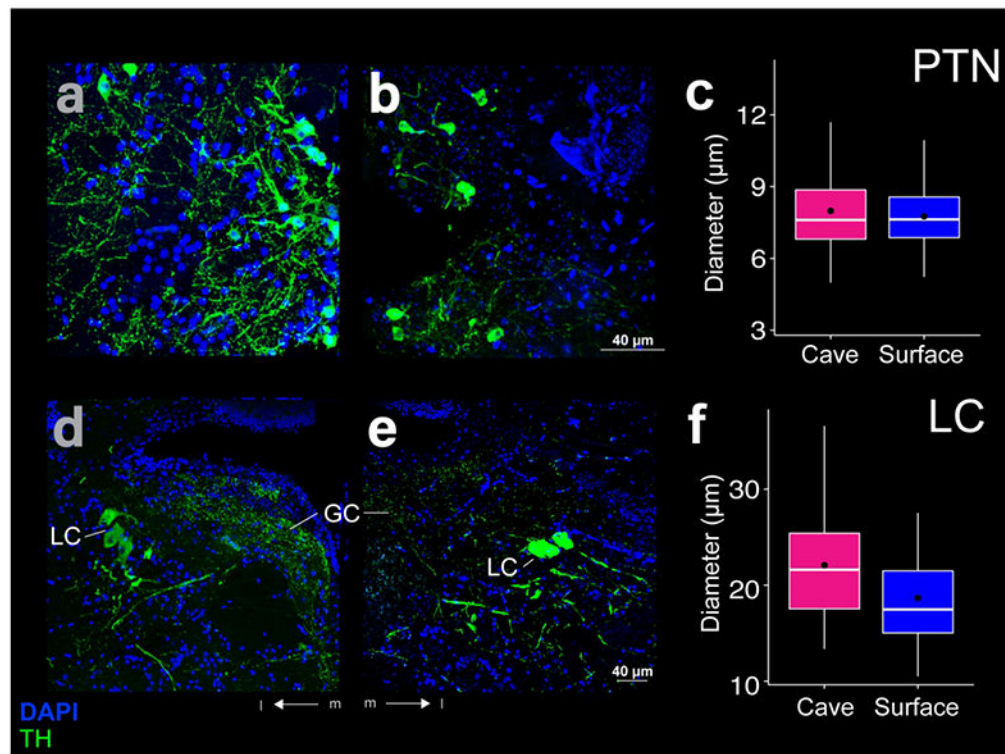
Figure 12:

THir (green) and DAPI (blue) stained coronal sections of cave (left; a, d) and surface (right; b, e) Astyanax. THir labeled somata had significantly larger (p < 0.001) diameters in cave Astyanax in the locus coeruleus (LC; d-f), but not in the posterior tuberal nucleus (PTN; a-c). The box plots in the right column (c, f) show the distributions of THir somata diameters of cave (pink) and surface (blue) Astyanax for that row. Black dots are the mean diameter, middle white line is the median, limits of the colored box indicate quartiles, and vertical white lines extend to the minimum and maximum diameters.